Adhesion and Signaling of Tumor Cells to Leukocytes and Endothelium in Cancer Metastasis

Cheng Dong

Abstract Heterotypic cell–cell adhesion in the near wall region under dynamic shear forces has been studied. In particular, we focus on neutrophil (PMN)–melanoma cell emboli formation in a non-linear shear flow and subsequent tethering to the vascular endothelium (EC) as a result of cell–cell aggregation. The extent of tumor cell adhesion to a vessel wall is governed by the kinetic formation/disruption of receptor–ligand bonds, soluble signaling proteins within the tumor microenvironment, and the hydrodynamic shear within the circulation. Upon tumor cell arrest on the endothelium, retraction of EC during tumor cell extravasation occurs due to the disruption of intercellular channels or disassembly of the vascular endothelial (VE)-cadherin homodimers that allow the passage of soluble proteins and cells. Preliminary studies have found tumor-elicited PMNs increase melanoma cell extravasation, which involves PMNs tethering on the EC and subsequently capturing/maintaining melanoma cells in close proximity to the EC. Results have indicated a novel finding that PMN-facilitated melanoma cell arrest on the EC is mediated by binding between the intercellular adhesion molecule (ICAM)-1 (expressing on both melanoma cells and ECs) and β_2 integrins on PMNs, influenced by tumor-induced inflammatory cytokines, e.g., interleukin (IL)-8, and hydrodynamic shear rates. Furthermore, the adherens junctions in terms of VE-cadherin are regulated by endothelial mitogen activated protein kinases (MAPK) in response to tumor cell adhesion to the EC, as well as to IL-8 and several other soluble signaling proteins within the tumor microenvironment. These studies will yield new evidence for the complex role of hemodynamics, protein signaling, and heterotypic cell adhesion in the recruitment of metastatic cancer

C. Dong (✉)
Department of Bioengineering, The Pennsylvania State University,
University Park, PA 16802, USA
e-mail: cxd23@psu.edu

Stud Mechanobiol Tissue Eng Biomater (2011) 4: 477–521
DOI: 10.1007/8415_2010_21

Published Online: 2 November 2010

cells to the EC in the microcirculation during metastasis, which will be significant in fostering new cross-disciplinary approaches to cancer treatment.

1 Introduction

Cancer is a complicated disease that requires the coordination of many different cellular processes. Metastasis is the spread of tumor cells (TC) from a primary tumor site to a secondary site and is the cause of most cancer related deaths. There are several pathways for a tumor to spread—through the vasculature or the lymph system to an adjacent organ. The studies presented here examine several possible mechanisms by which melanoma extravasation to secondary tumor sites occurs through the vasculature and how the inflammatory microenvironment may affect TC adhesion to and migration through the EC barrier under dynamic flow conditions from the circulation.

1.1 Tumor Cell Adhesion and Extravasation

Human leukocytes, including PMNs, actively participate in the inflammatory response via adhesion to the EC [89]. It has become evident from in vivo studies that the mechanisms utilized by leukocytes and metastatic tumor cells to adhere to a vessel wall prior to extravasation are very different [56]. One observation from in vivo video microscopy has indicated that tumor cells are trapped in capillaries and only arrest on the EC on the basis of vessel-size restriction in the microcirculation [8]. It has also been suggested that initial microvascular arrest of metastasizing tumor cells (from cell lines of six different histological origins) does not exhibit "leukocyte-like rolling" adhesive interaction with the EC [92]. In contrast, another in vivo study has discovered that the B16 melanoma cells could adhere to the walls of pre-sinusoidal vessels in mice pretreated with IL-1α [79]. They suggested that the release of inflammatory cytokines into the bloodstream could cause the arrest of melanoma cells in portal venules, by a chemoattraction and adhesion-mediated mechanism, rather than by a size restriction-only mechanism. Clearly these studies are somewhat contradictory and additional work is needed to characterize the event in TC adhesion to the EC, subsequent TC extravasation and metastasis.

Several ligands for inducible endothelial adhesion molecules have been identified on various types of tumor cells [103]. For example, Miele et al. [60] reported that a dose- and time-dependent increase in surface expression of ICAM-1 was found in human malignant melanoma cells. They also found that inhibiting ICAM-1 reduced melanoma lung metastasis in vivo. All these studies have supported an adhesive mechanism between TC and EC, rather than a simple mechanical entrapment, such as vessel-size restriction. Although melanoma cells express high

levels of ICAM-1, they do not express β_2 integrins (CD11a/CD18 or LFA-1; CD11b/CD18 or Mac-1), sLe^x or other sialylated molecules at levels to effectively adhere to the EC within the circulation [108]. An interesting study showed that PMNs and activated macrophages increased the ability of rat hepatocarcinoma cells to adhere to an EC monolayer [90]. In addition, tumor-elicited PMNs, in contrast to normal PMNs, were found to enhance metastatic potential and invasiveness of rat mammary adenocarcinoma cells in an in vivo tumor-bearing rat model [102]. Using light and electron microscopy, circulating PMNs were discovered in close association with metastatic TCs, including at the time of TC arrest [10]. These studies have clearly suggested that the immune system, and PMNs in particular, could affect tumor cell metastasis. However there is little understanding of tumor immunoediting and the adhesion mechanisms involved [4, 17, 41, 52].

1.2 Inflammatory Cytokines and Signaling

Chemokines represent a large family of polypeptide signaling molecules that are notable for their role in chemotaxis, leukocyte homing, and directional migration. Melanomas, and the cells derived from them, have been found to express a number of chemokines, including IL-8, growth-related oncogene (GRO)α-γ, and monocyte chemotactic protein (MCP)-1, which are implicated in melanoma cells themselves and the tumor infiltrating leukocytes [71]. Although several chemokines have been implicated in influencing adhesive properties of transformed cells, IL-8 is of particular interest. IL-8 has a wide range of pro-inflammatory effects, which mediate PMN migration from the circulation to sites of infection via activation of CXC chemokine receptors 1 and 2 (CXCR1/2) on PMNs [32, 65, 100]. IL-8 secretion is also a marker for increasing metastatic potentials, e.g., as an important promoter for melanoma growth [78, 83, 84]. Melanoma cells secrete IL-8 which alters adhesion molecule expression on PMNs [86]. IL-8 could potentially enhance PMN binding to melanoma cells and EC. In addition to IL-8, other factors such as IL-1β, IL-6, MCP-1, tumor necrosis factor (TNF)-α or GRO-α have also been shown to regulate immune responses and modulate tumor behavior [6, 63]. Chemokines or cytokines secreted by TCs and/or PMNs may play an important role in communication between melanomas and PMN and affect the interactions between them as well [25]. However, mechanisms regulating chemokine expression in a tumor microenvironment and roles played by endogenous chemokines in mediating TC extravasation from the circulation are unknown.

From in vitro models, interactions between ICAM-1 expressing cells and β_2 integrins on PMNs could potentially enhance melanoma cell adhesion to the EC mediated by PMN tethering, which further promote extravasation under dynamic flow conditions [53, 57, 87]. While IL-8 has been shown to promote melanoma angiogenesis and metastasis [2], involvement of PMNs in this process and mechanistic basis by which these cells could promote this process in vivo remains unclear. To dissect involvement of IL-8 secreted by melanoma cells and PMNs in

development of lung metastases, most recent mice studies by Huh et al. [36] showed that transient metastatic melanoma cells attached to PMNs in the lungs were significantly affected by high levels of IL-8. Secreted IL-8 increased β_2 integrin expressions (specifically Mac-1 molecules) on PMNs promoting tethering of ICAM-1 expressing melanoma cells to the EC via binding to the PMNs [52]. Therefore, Huh's in vivo work found that enhanced melanoma cells co-localization with PMNs increased the retention of TCs in the lungs resulting in enhanced trans-endothelial migration and subsequent metastasis development. Reducing expression of IL-8 using small interfering (si)RNA, decreased extracellular levels of IL-8 and Mac-1 expressions on PMNs, which reduced interactions between melanomas and PMNs. This resulted in fewer melanoma cells being tethered to the lung endothelium and retained in the lung thereby decreasing extravasation and metastasis development in vivo.

1.3 Cell Adhesion Kinetics

Cellular adhesion is mediated by the formation of receptor–ligand bonds. The combination of a receptor and a ligand that results in cellular adhesion can be considered as a chemical reaction. Kinetics is the study of the rates of chemical reactions and has been used to study cellular adhesion. The kinetics of leukocyte adhesion to the EC has been widely studied and various kinetic parameters of the molecules involved have been reported [1, 67, 88]. However, the kinetic mechanisms involved in melanoma cell adhesion, especially involving heterotypic cell–cell adhesion, have not been studied extensively and the steps leading to melanoma extravasation from the circulation are still poorly understood. As discussed earlier, melanoma cells have not been observed to roll along the EC similar to PMNs [92]. Previous investigations have determined that melanoma cells do not express selectin ligands or β_2 integrins at sufficient levels to mediate rolling or direct adhesive interactions with EC. Melanoma cells, however, do express ICAM-1, which can possibly bind to the integrins expressed by PMNs.

Resting PMNs express very few β_2 integrins in their high affinity states. Approximately 1,000 of the 15,000 expressed Mac-1 molecules and 9,000 of the 50,000 LFA-1 molecules expressed per cell are in a high affinity state before activation [82]. Many adhesion studies have shown that LFA-1 is more important for the initial tethering step of PMN adhesion to ICAM-1, whereas Mac-1 serves to stabilize already formed adhesions [29, 68]. For the interactions of LFA-1 with ICAM-1, a range of values have been determined for the dissociation rate under zero pulling force using different methods. Zhang et al. [109] calculated a dissociation rate of 0.17 s^{-1} using an LFA-1 expressing T-cell hybridoma line and immobilized ICAM-1 to perform atomic force microscopy and applying Bell's model [3]. A dissociation rate of 0.3 s^{-1} was estimated by Vitte et al. [97] using a parallel-plate flow chamber experiment utilizing Jurkat cells and immobilized ICAM-1, and Tominaga et al. [94] estimated a rate of 0.1 s^{-1} using a surface

plasmon resonance assay using soluble forms of both ICAM-1 and LFA-1. There is a higher variability in the association rates estimated using the different assays and cell types. Association rate estimates were calculated from the SPR assay as 200,000 M^{-1} s^{-1} [94] and from the parallel-plate flow chamber assay as 82 M^{-1} s^{-1} [97]. We therefore closely followed the method by Vitte et al. [97] in determining melanoma–PMN adhesion kinetic parameters.

1.4 Role of Fluid Dynamics Parameters

Under static in vitro conditions, melanoma cells do migrate through the EC. However, when they were exposed to a shear flow under stress 4 dyn/cm^2, the TC extravasation was found to be significantly decreased [86]. When PMNs were introduced to the TC suspension under the same shear conditions, 85% of the melanoma cell extravasation was recovered. This evidence has led to the hypothesis that PMNs may facilitate melanoma cell adhesion to and migration through the EC under flow conditions. Parallel-plate flow chamber experiments of TC–PMN aggregation under varying flow conditions showed fewer TCs adhered to the EC at higher shear rates [53]. As shear flow is always present in the body and these studies suggest that the properties of the fluid flow itself may influence the mechanism of melanoma cell adhesion and extravasation, especially when interacting with PMNs.

Fluid transport might govern flow-enhanced cell tethering [16, 110]. Results from a novel extravasation or a parallel-plate flow chamber have suggested that intercellular contact time, which is proportional to the inverse of wall shear rate, has a greater influence in the TC adhesion efficiency than the wall shear stress [50, 51, 58]. Wall shear stress (τ_w) and shear rate ($\dot{\gamma}$) are related by the definition $\tau_w = \mu\dot{\gamma}$ where μ is the viscosity of the fluid. If the magnitude of the fluid viscosity is increased and that of the shear rate is decreased proportionally, the shear stress remains constant. Several published experiments have been designed around this principle to distinguish the effect of the shear rate from that of shear stress [27, 76]. Under the same shear rate with varying fluid viscosity (or shear stress), no significant difference in the number of extravasated melanoma cells was observed; however, under a constant shear stress and decreasing shear rate, there was a significant increase in melanoma extravasation [87]. The same trends were observed for the aggregation of melanoma cells with PMNs in parallel-plate flow chamber experiments using the same variations in flow parameters [53]. These studies have suggested that TC arrest on the EC is a necessary step in PMN-mediated TC extravasation under flow conditions. This mechanism is regulated by hydrodynamic shear rates, which potentially affects TC–PMN contact time, revealing it is possibly convection driven. However, such fluid dynamics problems are not well studied, especially involving heterotypic cell adhesion in cancer.

Cell deformability has been shown to play an important role in affecting cell adhesion in a shear flow [5, 15, 35, 46]. Usually, an increase in shear force would

have a stronger tendency to detach a cell from its substrate or separate a cell from cell–cell aggregations; however, at the same time increasing shear stress also increases cell–cell contact areas due to the cell deformation that provides stronger adhesion. Therefore, hydrodynamics plays a complex role in the cell adhesion process.

1.5 Computational Fluid Dynamics and Cell Models

Computational fluid dynamics, or CFD, has been used to investigate the mechanisms involved in PMN adhesion to the EC. Numerical models of cellular in vitro systems have been created in order to determine effects of adhesion properties, fluid properties, and deformability on the efficiency of adhesion [37, 40, 66]. The majority of these models did not include a second (or heterotypic) cell type interacting with PMNs and ECs within the circulation; with the exception of Migliorini et al. [61], who modeled a red blood cell (RBC) colliding with a PMN. This is significantly different from modeling adhesion-specific TC–PMN interactions, due to the lack of specific RBC–PMN adhesion. A recent study developed by Hoskins et al. [34] extended these models by modeling TC interactions with a PMN adherent to the EC.

Currently the most sophisticated numerical models of PMN adhesion to the EC represent PMNs as 3-D deformable bodies with spring-type microvilli and adhesion molecules scattered on the membrane [37, 40, 66]. These models all employ membrane-tracking algorithms that do not discretize the outer membrane of the cells explicitly. These methods are less computationally intensive than an explicit method, but do not precisely resolve the location of the cell membrane or the fluid dynamics in the immediate vicinity of the cell membrane. Hoskins et al. [34] explicitly tracked the location of the deformable membrane and modeled the internal and external fluids separately. This will yield a more accurate representation of the cell deformation and fluid behavior.

The deformation of passive PMNs using the micropipette aspiration technique has been widely studied to determine material parameters of PMNs [19, 20, 104]. As PMNs traverse the circulation, they often encounter blood vessels with a smaller radius than the cell radius. Several in vitro experiments were used to recreate that situation [22]. Many numerical models have been developed which attempt to recreate the behavior of PMNs as they undergo the large deformations induced in the micropipette experiments [18, 23]. Although the deformation that will be modeled in the current work is less significant, the insight that has been gained by completing those studies can guide the modeling process.

Kunz et al. [44] have developed a CFD code, NPHASE, which has been developed, applied and validated for numerous single-phase and multi-phase flows. NPHASE incorporates several elements of modern CFD analysis including overset and unstructured meshes, parallel processing, fluid–structure interaction and moving/deforming meshes, each of which will be applied in the proposed cell

system modeling. In the current study, NPHASE will be applied in a DNS framework, where each cell in the system is explicitly resolved. The code has been specifically validated [34, 47] for the very low Reynolds number cellular system flows of interest here.

1.6 Endothelial Junction Adherence

Interendothelial adherens junctions account for the majority of barrier function of normal endothelium, and are responsible for regulating the passage of proteins and circulating cells [11]. Adherens junctions are characterized by the localization of VE-cadherin, a transmembrane protein, its cytoplasmic tail interacts directly with important cytoskeletal and signaling proteins, including α-actinin, α/β-catenin, plakoglobin, and actin [45]. VE-cadherin participates in most of the stages of transmigration of inflammatory cells. The loss of homophilic binding of VE-cadherins weakens the adhesive interaction between neighboring ECs, permitting transvascular cell penetration [12]. Homophilic binding activity of VE-cadherin is, in part, regulated by tyrosine-phosphorylation of its cytoplasmic tail [98], suggesting a direct role for protein tyrosine kinases in regulating interendothelial junctions, and subsequent transvascular cell migration.

Tumor cell-initiated signaling events that lead to changes in EC integrity have not been extensively characterized. High expression levels of $\alpha_4\beta_1$ integrin associated with highly metastatic melanoma cells is correlated with a marked increase in melanoma extravasation through endothelial layers [43, 81]. While several studies have focused on the effects of $\alpha_4\beta_1$ and vascular adhesion molecule-1 (VCAM-1) interactions on metastasis and adhesion of melanoma cells to the endothelium [26, 48, 75, 77, 99], recent studies have found that these adhesion events lead to the disassembly of VE-cadherin which facilitates melanoma transendothelial migration [39, 72, 73]. However, melanoma cells themselves secrete large amounts of soluble proteins including IL-8, IL-6, IL-1β, and GRO-α. Melanoma cells with high metastatic potential have been shown to secrete higher amounts of IL-8 [70, 74]. These results were further supported by in vivo studies showing an overall decrease in tumorigenicity and metastasis when mice lacking CXCR2 (the receptor for IL-8) were injected with melanoma cells [85].

Peng et al. [73] monitored the $[Ca^{2+}]_i$ in human umbilical vein endothelial cells (HUVEC) following contact with human melanoma cells. They showed that transient rise in endothelial $[Ca^{2+}]_i$ was elicited specifically by melanoma cells, and this response recruited the classical $[Ca^{2+}]_i$ release mechanism via pertussis toxin (PT)-sensitive G proteins in the EC. In addition, they demonstrated that the loss of VE-cadherin integrity in EC appeared at the interendothelial border in response to melanoma cell contacts. The regulation of melanoma cell-mediated junctions was independent of tyrosine phosphorylation of VE-cadherin. Most importantly, melanoma cells induced junction disassembly in the manner strongly

related to phospholipase C (PLC) activation, since inhibition of PLC significantly reduced the disruptions of VE-cadherin by melanoma cells. Phosphatidylinositol-3-kinase (PI3K), however, was not responsible for the melanoma cell-associated VE-cadherin redistribution. In addition, melanoma cell transendothelial migration was diminished in the absence of PLC or PI3K activity. These findings suggest an involvement of PLC in endothelial signaling pathways recruited by melanoma cells in breaching the vasculature.

It is well established that p38 MAPK activation plays a key role in the initial break down of VE-cadherin junctions to facilitate cell migration through the EC [69, 95]. Some recent studies have shown that the VCAM-1 receptor on the endothelium induces intercellular gap formation through the Rho-like GTPase Rac1 signaling that results in activation of p38 MAP kinase proteins further downstream of the Rac pathway [39, 96]. The question remains as to whether melanoma cells trigger VE-cadherin disassembly primarily through cell–cell contact mediated events or through soluble protein events. Furthermore, could these tumor-induced events modulate specific intracellular pathways in the endothelium leading to disassembly of VE-cadherin homodimers?

2 Experimental Materials and Methods

2.1 Cell Preparation

Human melanoma cell lines WM35 and WM9 were provided by Dr. Meenhard Herlyn (Wistar Institute, Philadelphia, PA, USA) and maintained in Roswell Park Memorial Institute 1640 medium (RPMI 1640; Biosource, Inc., Camarillo, CA, USA) supplemented with 10% fetal bovine serum (FBS; Biosource, Inc.) and 100 units/ml penicillin–streptomycin (Biosource, Inc.) at 37°C under 5% CO_2. 1205Lu cells (from Dr. Gavin P. Robertson, Penn State Hershey Medical Center, Hershey, PA, USA) and C8161 cells (from Dr. Danny Welch, University of Alabama, Birmingham, AL, USA) were cultured respectively in Dulbecco's Modified Eagle's Medium (DMEM) and DMEM-F12 (Biosource, Inc.) supplemented with 10% FBS in a standard cell culture condition (5% CO_2/37°C). Correlation of tumor metastatic potentials with melanoma cell invasiveness, chemotactic migration and adhesiveness is shown in Table 1.

Fibroblast L-cells that had been transfected to express human E-selectin and ICAM-1 (EI cells) were provided by Dr. Scott Simon (University of California, Davis, CA, USA), which were maintained in culture as described elsewhere [27]. The EI cells were used in our initial experiments as a model of an endothelial monolayer for studying TC–EC, PMN–EC, and TC–PMN–EC adhesion.

Human umbilical vein endothelial cells were obtained from American Type Culture Collection (ATCC) (Manassas, VA, USA) and maintained in F12-K medium with 10% FBS, 30 μg/ml of EC growth supplement, 50 μg/ml heparin

Table 1 "Metastatic" potential was qualitatively determined from the cell line origin; "Chemotactic" potential was measured by cell static migration toward soluble type IV collagen (CIV; 100 μg/ml) using Boyden chamber; and "Adhesion" potential was quantified by comparing relative mean fluorescence levels of ICAM-1 expression obtained by flow cytometry

Cell line	Potentials			References
	Metastatic	Chemotactic (CIV)	Adhesion (ICAM-1)	
1205Lu	++++	+++	+++	[80]
C8161	+++	++	++	[101, 106]
WM 9	++	++	+++	http://www.wistar.upenn.edu/herlyn/melcell.htm
A2058	+	++	++	[14]
WM35	−	+	+	http://www.wistar.upenn.edu/herlyn/melcell.htm

(Mallinckrodt Baker, Inc.), 100 units/ml of penicillin–streptomycin (Biofluids, Inc.) [39, 73].

Fresh human blood was drawn from healthy donors under informed consent as approved by the Pennsylvania State University Institutional Review Board. PMNs were separated from blood using Ficoll-Hypaque (Histopaque; Sigma Chemical Co.). After centrifugation at 620*g* for 30 min, PMNs were carefully isolated and suspended in Dulbecco's phosphate-buffered saline (DPBS) with 0.1% human serum albumin (HSA; Sigma Chemical Co.). Erythrocytes were lysed using ACK lysis buffer (0.15 M NH_4Cl, 10 mM $KHCO_3$, 0.1 mM Na_2EDTA; [pH 7.4]) and removed. The cells were washed and resuspended in 0.1% HSA/DPBS, and gently rocked until they were used in experiments. The cell preparations were 99.5% pure PMNs, as analyzed by a Diff-Quick stain (Dade Behring Inc., Newark, DE, USA). PMNs were resuspended in RPMI 1640 medium supplemented with 5% FBS and cultured with or without melanoma cells.

For PMN and melanoma cell co-culture, PMNs were added to the confluent melanoma cells, either directly or separated by a Transwell insert with 0.4 μm pore size. In some experiments, PMNs or ECs were stimulated with recombinant human IL-8 (12.5, 25 or 125 ng/ml), IL-1β (5, 10 or 25 ng/ml), IL-6 (50 or 100 ng/ml), GRO-α (100 or 200 ng/ml) (Biosource, Inc.) or a combination of IL-8, IL-1β, IL-6 and GRO-α cytokines with chosen concentrations, respectively.

2.2 Tumor Conditioned Medium

Selected melanoma cells were cultured in 75 cm^2 flasks under growth conditions described above to 90–95% confluency, after which medium was aspirated and replaced with fresh 5 ml of RPMI (for WM35 cells) or DMEM (for A2058 and 1205Lu cells) with 2% FBS. The medium was then removed after a 24-h period of chosen tumor cell culture and centrifuged in 50 ml conical tubes at 1,500 rpm at 4°C for 5 min to remove any remaining cells.

2.3 Small Interfering RNA (siRNA) Targeting IL-8

SiRNA (100 pmol) was introduced into 1.0×10^6 1205Lu, C8161.Cl9 via nucleofection using an Amaxa Nucleofector using Solution R/program K-17 [52, 80]. Transfection efficiency was >95% with 80–90% cell viability [80]. Following siRNA introduction, cells were allowed to recover for 2 days and then replated in 96-well plates. Five days later, cell viability was measured using the MTS assay (CellTiter 96 AQueous Cell Proliferation Assay, Promega, Madison, WI, USA).

Duplexed Stealth siRNA (Invitrogen, Carlsbad, CA) were used for the IL-8 studies. The following siRNA sequences were used for targeting IL-8 [36]. *IL-8#1*: GCA GCU CUG UGU GAA GGU GCA GUU U, *IL-8#2:* CCA AGG AGU GCU AAA GAA CUU AGA U.

2.4 Western Blots

Cells were collected and washed with cold PBS, then whole cell extracts were prepared by resuspending cells in lysis buffer (10 mM Tris–HCl [pH 7.4], 150 mM NaCl, 1 mM EDTA [pH 8.0], 2 mM Na_3VO_3, 10 mM NaF, 10 mM $Na_4P_2O_7$, 1% NP-40, 1 mM PMSF, 2 ng/ml pepstatin A). Lysates were incubated on ice for 30 min followed by a centrifugation at 16,000*g* for 1 min at 4°C. The pellet was discarded and the supernatant was mixed with 2× SDS running buffer (0.2% bromophenol blue, 4% SDS, 100 mM Tris [pH 6.8], 200 mM DTT, 20% glycerol) in 1:1 ratio. Samples were boiled for 3 min and 15 μl were loaded onto a 12 or 15% SDS-PAGE gel and proteins were transferred to a 0.2 μm PVDF membrane (Millipore Co., Billerica, MA, USA) by electroblotting. Primary antibodies included rabbit anti-human IL-8 (Biosource, Inc.) and anti-β-actin IgG1 (Sigma Chemical Co.). Secondary antibodies were peroxidase-conjugated goat anti-rabbit IgG or goat anti-mouse IgG. Proteins were detected using the Enhanced Chemiluminescence Detection System (Amersham Pharmacia Biotech, Arlington Heights, IL, USA).

2.5 Enzyme-linked Immunosorbent Assays

At the end of assays, cell-free supernatants were collected by a centrifugation at 430*g* for five minutes and stored at −80°C until Enzyme-linked immunosorbent assays (ELISA) was performed. ELISA detection of protein secretion was performed at the Pennsylvania State University NIH Cytokine Core Lab. Mouse anti-human capture antibody to specific target chemokine or cytokine was diluted to 2 μg/ml in coating buffer (0.1 M $NaHCO_3$ [pH 8.2]) and 50 μl was added to each well of the 96-well ELISA plate for overnight incubation at 4°C. The plate was

then washed four times with 20% Tween 20 in phosphate-buffered saline (PBST) [pH 7.0] and blocked with 1% BSA in PBS for 2 h at room temperature. 100 µl target chemokine or cytokine standards and samples were added to each well for overnight incubation at 4°C. The plate was washed four times next day and 100 µl of 0.2 µg/ml biotinylated affinity purified goat anti-human polyclonal detection antibody was added to each well, followed by 2 h incubation at room temperature. The plate was then washed six times and incubated with 10 µl streptavidin peroxidase (1 µg/ml, Sigma Chemical Co.) for 30 min at room temperature. 100 µl of 2,2′-Azino-bis (3-ethylbenzothiazoline-6-sulfonic acid) diammonium salt (Sigma Chemical Co.)/peroxide substrate solution was then added for 1 h in the dark. The plate was read using a microtiter plate reader (Packard, Downers Grove, IL, USA) at a wavelength of 405 nm.

2.6 Flow Cytometry

The cells of interest were treated with murine anti-human CD marker primary antibodies (e.g., anti-CD11a, anti-CD11b, or anti-ICAM-1; 1 µg Ab/10^6 cells) (CalTag Laboratories) for 30 min at 4°C. The cells were then treated with secondary antibody, FITC-conjugated goat anti-mouse IgG $F(ab)_2$ fragment (1 µg/10^6 cells) (Jackson ImmunoResearch, West Grove, PA, USA) for 25 min at 4°C. In the case of blocking CXCR1 and CXCR2 receptors on PMNs, PE-conjugated anti-CD11b (1 µl/10^6 cells; CalTag Laboratories) was used to avoid binding secondary antibody to the existing CXCR1 and CXCR2 antibodies. The samples were fixed with 2% formaldehyde (Sigma) and analyzed using a Coulter EPICS XL (Coulter Corp., Fullerton, CA, USA) flow cytometer. Control cases used to determine background fluorescence were samples treated with secondary antibody only or PE-conjugated isotype control (CalTag Laboratories).

2.7 In vitro Flow Extravasation Assays

A flow extravasation assay was performed in a modified 48-well chemotactic Boyden chamber consisting of a top and bottom plate separated by a gasket. In brief, a 7 cm × 2 cm opening cut from the center of a 0.02 inch-thick gasket between top and bottom plates forms the flow field (Fig. 1; top right). The wall shear stress (τ_w) is related to the volumetric flow rate (Q) by $\tau_w = 6\mu Q/wh^2$, where μ is the fluid viscosity, h is height and w is width of the flow field. EI cells, which had been transfected from fibroblasts to express human E-selectin and ICAM-1, were used as a substrate for cell adhesion and as a model of an endothelial monolayer. E-Selectin and ICAM-1 levels were periodically checked by flow cytometry to verify expression level. ICAM-1 levels on EI cells were shown to be comparable with IL-1β stimulated HUVECs [27]. Hence, a monolayer was formed

by growing EI cells to confluence on sterilized PVP-free polycarbonate filters (8-μm pore) coated with fibronectin (30 μg/ml) [86]. The bottom side of the filter was scraped prior to use to remove any potential cell growth. Soluble type IV collagen (CIV; 100 μg/ml), which has been shown to induce melanoma cell chemotaxis [30, 31], was chosen as the chemoattractant in the center 12 wells. Typical experiments involved cases such as: PMNs; melanoma cells (respective cell lines with varied metastatic phenotypes from Table 1); PMNs + selected-type melanoma cells (5×10^5 cells of each cell type). The entire flow-migration assay was conducted in a 37°C, 5% CO_2 incubator for 4 h. To quantify migration, the filter was removed from the chamber and immediately stained with HEMA-3 (Fisher Scientific). The cells on the bottom side of each filter were imaged. No cells were found in the attractant wells after 4-h of migration. Three pictures were taken of each filter in different locations. The number of cells migrated was quantified/averaged for each filter. A minimum of three filters were analyzed for each data point. Background migration was subtracted from each sample as appropriate. Control experiments showed no PMNs migrated toward CIV.

2.8 Parallel-plate Flow Assays

Cell collision and adhesion experiments were performed in a parallel-plate flow chamber (Glycotech, Rockville, MD, USA) mounted on the stage of a phase-contrast optical microscope (Diaphot 330, Nikon, Japan). A syringe pump (Harvard Apparatus, South Natick, MA, USA) was used to generate a steady flow field in the flow chamber. A petri dish (35 mm) with a confluent EI cell monolayer was attached to the flow chamber [53]. All experiments were performed at 37°C. The field of view was 800 μm long (direction of the flow) by 600 μm. The focal plane was set on the EI monolayer. The flow chamber was perfused with appropriate media over the EI monolayer for 2–3 min at a shear rate of 40 s^{-1} for equilibration before the introduction of a predetermined concentration (1×10^6 cells/ml) of PMNs and WM9. PMNs were stimulated with 1 μM fMLP for 1 min or 1 ng/ml IL-8 for 1 h before the perfusion into parallel-plate flow chamber. After allowing PMNs and WM9 cells to contact the EI monolayer at a shear stress of 0.1–0.3 dyn/cm^2 for 2 min, we adjusted the shear stresses to the experimental range of 0.6–2 dyn/cm^2 and kept constant for 6–7 min. Experiments were performed in triplicate and analyzed off-line.

2.9 Animal Studies

Animal experimentations were performed according to protocols approved by the Institutional Animal Care and Use Committee at the Pennsylvania State University College of Medicine [36, 52, 80].

Tumor formation was measured in athymic-Foxn1^{nu} nude mice purchased from Herlan Sprague–Dawley (Indianapolis, IN, USA). 500 pmol of siRNA was nucleofected into 5.0×10^6 cells and after 48 h of recovery, 1.0×10^6 cells were collected in 0.2 ml of 10% FBS-DMEM to inject subcutaneously above both the left and right rib cages of 4–6 week old female mice. Dimensions of developing tumors were measured on alternate days using calipers.

To characterize in vivo interactions of melanoma cells with human PMNs, 100 pmol of siRNA were nucleofected into 1.0×10^6 GFP-tagged 1205Lu. After 36 h 0.5×10^6 cells in 0.2 ml of HBSS were collected. PMNs were isolated and were stained with CellTracker Orange CMTMR (C2927, Invitrogen, Carlsbad, CA, USA) according to manufactures protocol. Melanoma cells were injected i.v. into the left lateral tail vein of athymic-Foxn1^{nu} nude mice and human PMNs were injected i.v into the right lateral tail vein of nude mice. After 24 h, mice were sacrificed, lungs removed and analyzed for melanoma cells interacting with PMNs using Nikon SMZ 1500 dissecting microscope with fluorescence detection capabilities (for GFP; ex470/em500, for CellTracker Orange CMTMR; ex550/em600). Percentages of melanoma cells co-localized with PMNs were counted in fields where melanoma cells and PMNs coexisted [36].

To study mouse experimental metastasis, 100 pmol of siRNA were nucleofected into 1.0×10^6 GFP-tagged 1205Lu and C8161.Cl9 cells. After 36 h 0.5×10^6 cells in 0.2 ml of HBSS were injected i.v. into the lateral tail vein of nude mice. Mice were sacrificed 18 days later, necropsied, and lungs analyzed for presence of fluorescent metastases using a Nikon SMZ 1500 dissecting microscope with a Plan Apo 1.6× objective. Images were photographed at 48× magnifications from the ventral surface of each lung and number of fluorescent metastases as well as area occupied by metastases scored in pixels using IP lab imaging software (Scanalytics, Fairfax, VA, USA).

2.10 Statistical Analysis

All results are shown using mean ± standard error of the mean (SEM) unless otherwise stated. One-way ANOVA analysis was used for multiple comparisons and *t* tests were used for comparisons between two groups. $P < 0.05$ was considered to be significant.

3 Computational Models

3.1 Diffusion and Convection of Solutes in a Shear Flow

A two-dimensional Couette flow model was used to simulate the transport of IL-8 released by tumor cells in the circulation. The inputs used in the model are tabulated in Table 2.

Table 2 Description and source of variables as inputs for Comsol simulation

Variable	Description	Value	Source
Q	Volumetric flow rate	0.025 ml/min, 0.04 ml/min and 0.08 ml/min	Experimental setting
D_{AB}	IL-8 diffusion coefficient	2.59×10^{-10} m^2/s	[62, 107]
C_0	IL-8 secreted by a melanoma cell	Liang et al. [51]	Detected using ELISA from medium collected after flow assay
a	Distance from the center of channel to the wall	63.5 μm	Parallel plate chamber geometry
ρ	Density of fluid	1.0×10^3 kg/m^3	Known constant
u	Melanoma cell velocity	9.046×10^{-5}, 1.447×10^{-4}, 2.894×10^{-4} m/s	Calculated from Eqs. 3 and 4
μ	Viscosity	1.0, 2.0, 3.2 cP	Experimental setting

IL-8 distribution under flow conditions was modeled computationally using the commercial software package Comsol Multiphysics 3.2 (Comsol, Stockholm, Sweden), which employs a finite element method to solve the governing partial differential equations. To simulate the IL-8 transport, the convection and diffusion application mode was selected and the Navier–Stokes application mode was used to calculate the velocity pattern. The convection–diffusion equation solved is shown in Eq. 1:

$$\frac{\partial c_i}{\partial t} + \nabla(c_i u) = D_i \nabla^2 c_i, \tag{1}$$

where c_i is the IL-8 concentration, u is the velocity, and D_i is the solute diffusion coefficient. The diffusion coefficient for IL-8 was obtained from literature [62]. It has been shown that for small proteins, the diffusion coefficient is proportional to molecular weight [105, 107]. A constant flux was assigned at the cell surface and complete dilution was assumed very far from the cell; mathematically stated as:

$$c = C_0 \text{ at } r = R \quad \text{and} \quad c \to 0 \text{ as } r \to \infty$$

where C_0 is the IL-8 concentration and R is the tumor cell radius. It was assumed that the secreted IL-8 would not be re-consumed by the secreting tumor cell and C_0 be uniform over the surface of the cell.

The velocity profile was calculated using the Navier–Stokes application mode, which solves the incompressible momentum and mass conservation:

$$\begin{aligned} &\rho \frac{\partial u}{\partial t} + \rho(u \cdot \nabla)u + \nabla p - \mu \nabla^2 u = 0 \\ &\nabla \cdot u = 0 \end{aligned} \tag{2}$$

where u is the velocity, ρ is the density of fluid, μ is the viscosity and p is the pressure. The fluid was assumed to be Newtonian, incompressible, steady and laminar. A no-slip boundary condition was implemented at the channel walls. Uniform velocity and constant pressure were prescribed at the inlet and outlet, respectively. In the fully developed region, the classical parabolic velocity profile (Poiseuille flow) was obtained. The velocity at a given location in the chamber can be calculated from the equation below:

$$u = \left(\frac{\Delta P a^2}{4\mu L}\right)\left[1 - \left(\frac{r}{a}\right)^2\right] \tag{3}$$

where the $\Delta P/L$ is the driving force, r is the distance from the center of the channel to the location, μ is the viscosity, and a is the distance from the center of the channel to the channel wall. The driving force, $\Delta P/L$, can be derived from the equation:

$$\frac{\Delta P}{L} = \frac{8\mu Q}{\pi a^4} \tag{4}$$

where Q is the volumetric flow rate.

The relation between diffusion coefficient and solvent viscosity can be calculated using the Stokes–Einstein equation as follows.

$$D_{AB}\mu_B = \frac{k_b}{6\pi R_A} \tag{5}$$

where D_{AB} is the diffusion coefficient of solute A in solvent B, R_A is the hydrodynamic radius of solute A, k_b is Boltzmann's constant, T is the Kelvin temperature, and μ_B is the solvent viscosity. Note that the Stokes–Einstein equation usually gives poor accuracy when solute A is a large molecule. Recently, a modification of the Stokes–Einstein equation for small molecules was proposed by Kooijman [42]. However, both equations have shown that the diffusion coefficient is inversely proportional to the solution viscosity.

3.2 Receptor–ligand Binding Association Rate

A molecular model of receptor–ligand binding has been developed and used in simulations of cell–cell adhesion [13]. In this model, the association rate, k_{on}, governs the likelihood of a receptor to form a bond with a ligand on another cell, whose equation is shown in Eq. 6:

$$k_{on} = A_L(n_L - n_B)k_{on}^0 \exp\left(\frac{-\sigma_{ts}(\varepsilon - \lambda)^2}{2k_bT}\right) \tag{6}$$

where A_L is the surface area on a ligand-bearing cell that is available to a receptor, n_L is the number of ligands on a cell, n_B is the number of bonds already formed. These values and the separation distance between two cells, ε, are determined by the geometry and properties of a chosen cell. The association rate for the receptor–ligand binding under zero-force conditions, k_{on}^0, was determined for LFA-1 and Mac-1 binding with ICAM-1 in a companion effort [33]. The bond spring constant, σ_{ts}, and equilibrium length, λ, as well as the Boltzmann's constant, k_b, were assigned values found in the literature [13].

3.3 Melanoma–PMN Adhesion to the EC in a Shear Flow

A 3D model of a PMN and a tumor cell in flow has been developed in a companion effort to simulate the adhesion of a melanoma cell to a tethered PMN under flow conditions [34]. The model is used here to compare the force exerted on a melanoma cell, bound to a stationary PMN via a single bond, under varying flow conditions. Since bond formation is a random occurrence, which is based on the proximity of cells, receptor and ligand surface densities and locations, and molecular properties, bonds may form in any position between a melanoma cell and a PMN. Here, a direct comparison of bond force time history in various flow conditions is desired; thus the same initial location was assumed for the melanoma cell and the single bond in all simulations.

One stationary, adherent PMN was modeled on the bottom plate of the parallel plate flow chamber geometry and a free stream tumor cell was modeled above and slightly upstream of the PMN in the flow [51]. A single bond, treated as a linear bond spring, was seeded between the two cells. The forces on the tumor cell due to the fluid and the bond were used to calculate the cell motion.

Two commercial codes were used to simulate the two cell system. Harpoon (Sharc, Manchester, UK) automatically generates the computational grids, and AcuSolve (ACUSIM Software, Mountain View, CA, USA) calculates the flow profile and force distributions. The cell motion calculation was completed by Kunz-developed Python script[44], which also controls the overall simulation. The order of operations controlled by the script was described in details from Hoskins et al. [34].

Harpoon is a grid generator that creates hexahedra-dominant meshes in a very short time. In the simulations used in this study, a new grid was generated at each time step with the new tumor cell location.

AcuSolve is an incompressible flow solver based on the Galerkin/Least Squares finite element method (GLS). The steady, incompressible Navier–Stokes and continuity equations were solved, as shown in Eq. 2. Variables are also as defined for Eq. 2.

The solution of Newton's Second Law, shown in Eq. 7, governed the spherical tumor cell motion.

$$\frac{d^2\vec{x}}{dt^2} = \frac{\vec{F}}{m}$$
$$\frac{d^2\vec{\theta}}{dt^2} = \frac{\vec{\tau}}{I} \quad (7)$$

where $\vec{x}$ and $\vec{\theta}$ are the tumor cell translations and rotations, $\vec{F}$ and $\vec{\tau}$ are the force and torque vectors on the tumor cell and m and I are the cell's mass and mass moment of inertia. These equations were solved assuming the tumor cell is a rigid body.

To represent the interactions between the microvilli on the cells' surfaces, a repulsion force with the form of a non-linear spring force, as shown in Eq. 8, was applied to the tumor cell.

$$F_{rep} = -kd + bd^3 \quad (8)$$

where k and b are constants and d is the distance between the cells. This force was applied along the normal to the PMN surface at the point of minimum separation distance between the cells. The line of the normal does not generally go through the center of the tumor cell, thus a torque is also applied.

4 Results

4.1 PMN-facilitated Tumor Cell Extravasation under Flow Conditions

An in vitro extravasation model (Fig. 1) was developed using a modified 48-well chemotactic "flow-migration" Boyden chamber [86].

The "PMN tethering frequency" was determined experimentally as the number of PMNs that adhered to the EC per unit time and area using a parallel-plate flow chamber (Fig. 1, bottom), including both rolling and firmly-arrested cells [53]. This frequency was normalized by cell flux to the surface to compensate for the different concentration of cells passing the same area of substrate at different shear rates. This normalization followed the procedure of Rinker et al. [76] based on equations derived by Munn et al. [64]. Melanoma–PMN aggregation on the EC was subsequently analyzed. Quantification started at the onset of experimental shear rate ($t = 0$ min) and lasted for 5 min. Aggregates could be characterized by differences in cell sizes and velocities (Fig. 1, bottom). Aggregation variables to be quantified included: the total number of tethered PMNs; number of collisions of melanoma cells (from the free stream near the EC) to tethered PMNs; aggregation of melanomas with tethered PMNs as a result of the collision; and final attachment of melanoma–PMN aggregates on the EC. For some cases in which more than one melanoma cell adhered to a PMN, we count such a case as two aggregates if two melanoma cells adhered to a PMN.

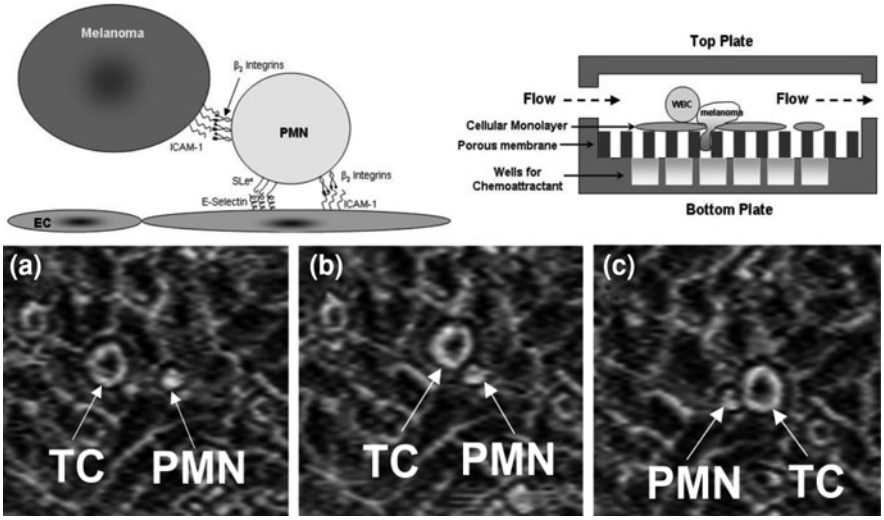

Fig. 1 Schematic of PMN-facilitated melanoma adhesion to the EC in a shear flow. *Top left* a melanoma cell in close proximity to the EC (using the EI cell model) via a tethered PMN. Melanoma cells are captured/retained by tethered PMN on the EI via β_2 integrins/ICAM-1 interactions. *Top right* cross-section view of the flow-migration chamber. *Bottom* representative aggregation of melanoma tumor cells (*TC*) to tethered PMN on an endothelial monolayer. Flow direction is from *left* to *right*: **a** a melanoma cell and a PMN on the monolayer at 0 s, **b** collision between a PMN and a melanoma cell after 20 s, and **c** arrest of a melanoma cell to the monolayer due to the formation of PMN–melanoma aggregates after 30 s

"Melanoma adhesion efficiency" was expressed by the following ratio [53]:

$$\text{Melanoma adhesion efficiency} = \frac{\text{Number of melanoma cells arrested on the monolayer}}{\text{Number of melanoma collisions to PMNs}}$$

where, the numerator is the number of melanoma cells arrested on the EI at the end of the entire flow assay as a result of collision between entering melanoma cells and tethered PMNs. The denominator is the total number of melanoma–PMN collisions near the EI surface counted as a transient accumulative parameter throughout the entire flow assay.

As a negative control, non-metastatic melanocyte migration was first tested under the static condition and found to be at a background level (Fig. 2a, bottom). In comparison, highly-metastatic C8161 and WM9 cells were more actively migratory under the no-flow condition than low-metastatic WM35 cells (Fig. 2a, "Static"). When exposed to a shear flow ($\sim$0.4 dyn/cm^2), extravasations of C8161, WM9 and WM35 cells toward CIV were all significantly less than those under static conditions (Fig. 2a), at a level similar to the melanocyte case. Addition of PMN to the melanoma cell suspension significantly enhanced tumor

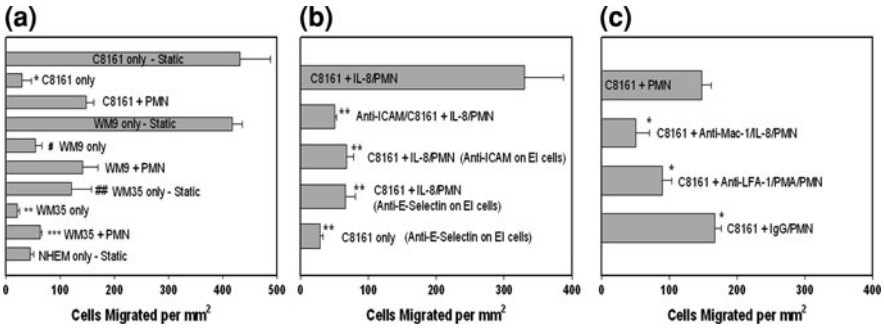

Fig. 2 **a** PMN affects C8161, WM9 and WM35 cell migration under shear conditions. NHEM are non-cancerous melanocyte used as a negative control. All cases were under a flow shear stress at 0.4 dyn/cm^2, unless labeled "Static" ($^*P < 0.01$ with respect to C8161 static case, $^{\#}P < 0.05$ with respect to WM9 static case, $^{**}P < 0.01$ with respect to WM35 static case, $^{\#\#}P < 0.05$ with respect to both C8161 and WM9 static cases, and $^{***}P < 0.02$ with respect to both C8161 + PMN and WM9 + PMN cases). **b** ICAM plays an important role in PMN-facilitated melanoma cell migration. The *second bar* shows disrupting C8161–PMN aggregation by blocking ICAM-1 on melanomas significantly reduces melanoma cell migration (PMNs were activated by IL-8). The *third* and *fourthbars* show inhibiting IL-8-stimulated PMN adhesion to the endothelium by blocking E-selectin or ICAM-1 on the EI also decreases C8161 cell migration ($^{**}P < 0.01$ with respect to C8161 + IL-8/PMN case at 0.4 dyn/cm^2). **c** Differential role of LFA-1 and Mac-1. Both Mac-1 and LFA-1 (to lesser degree) contribute to PMN-mediated melanoma extravasation. The *last bar* shows migration with isotype antibody-treated PMNs, as a control ($^*P < 0.05$ with respect to C8161 + PMN case at 0.4 dyn/cm^2). All the values are mean ± SEM for $N \geq 3$

cell extravasation under shear conditions compared with melanoma cells only (all P values < 0.05). Obviously, tumor metastatic potential correlates with melanoma cell extravasation behavior.

Figures 2b, c indicate that each binding step between EC, PMNs and melanoma cells affects tumor cell extravasation under flow conditions. ICAM-1 was functionally blocked on the C8161 cells and EI cells, respectively. Functionally blocking of ICAM-1 on C8161 cells or EI cells significantly reduced melanoma extravasations. Blocking E-selectin on the EI cells reduced C8161 melanoma cell migration by 80% compared with the C8161 + IL-8-activated PMN case (Fig. 2b). However, blocking E-selectin on the EI cells without PMN did not really change melanoma extravasation (Fig. 2b, bottom). To investigate whether PMN–melanoma interactions are mediated by receptor–ligand binding via β_2 integrins (on PMN) and ICAM-1 (on melanoma cells), melanoma cell extravasations were assayed in the presence of PMNs, in which CD11a (for LFA-1) and CD11b (for Mac-1) on PMNs were inhibited respectively with blocking antibodies. Blocking CD11b resulted in the greatest reduction in C8161 migration (66% reduction as compared to C8161 + PMN under 0.4 dyn/cm^2 shear stress; Fig. 2c). Similar results are shown that migration of melanomas was decreased by 40% in the presence of CD11a-blocked PMN.

4.2 Shear Rate Mediated Fluid Convection Affects PMN-Facilitated Melanoma Arrest on the EC

Using dextran to vary the medium viscosity (μ) of the cell suspension, either shear rate ($\dot{\gamma}$) or shear stress ($\tau = \mu\dot{\gamma}$) was held constant while the other was varied in order to determine how fluid shear impacts melanoma cell extravasation. We used ultra-high molecular weight dextran (2×10^6 MW) to avoid potential shielding effects [76] and to achieve a range of media viscosities from 0.7 cP (0% dextran) to 7.0 cP (4% dextran). Control experiments showed 0–4% dextran did not affect cellular adhesion molecule expression or media osmolarity [87]. Cases in which shear stress was held constant and shear rate varied from 55.5 to 555 s^{-1} yielded dramatic variation in C8161 cell extravasation (183 ± 24 cells per mm^2 at 555 s^{-1} to 290 ± 37 cells per mm^2 at 55.5 s^{-1}) that was inversely proportional to the shear rate ($P = 0.041$; Fig. 3a). In contrast, cases in which shear rate was held constant and shear stress ranged from 0.4 to 18 dyn/cm^2 resulted in C8161 migration levels that were not statistically different (Fig. 3b, c). These results suggest that PMN-facilitated migration of melanoma cells is affected by local hydrodynamic convection (which is inversely proportional to cell–cell adhesion contact time), not by the shear stress (which is proportional to fluid force).

To examine how PMN–C8161 cell aggregates adhere to the EI cell monolayer, the PMN tethering frequency was quantified using a parallel-plate flow chamber [53] at 3 shear rates (62.5, 100 and 200 s^{-1}) and 3 media viscosities (1.0, 2.0 and 3.2 cP). As seen in Fig. 4a, the PMN tethering frequency was significantly affected by both shear rate and shear stress. All frequencies were corrected for the decrease in cell flux with increasing shear rate and viscosity, and normalized against the lowest shear stress case. These results are different from the PMN-mediated C8161 migration and tumor adhesion efficiency results shown in Fig. 4b, c. As we see, melanoma *extravasation* and *adhesion efficiency* mediated by PMNs were both affected only by the shear rate, not the shear stress.

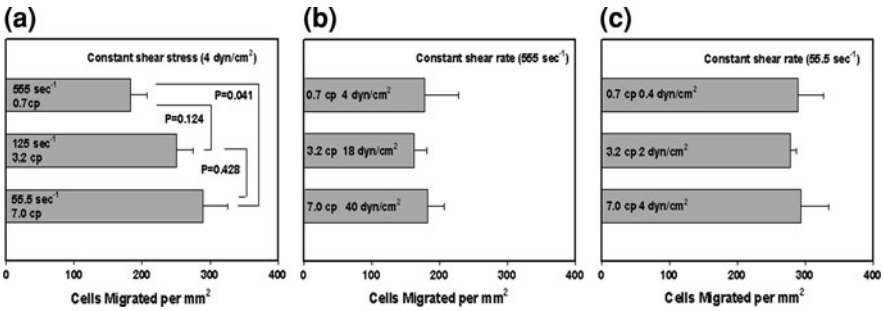

Fig. 3 Shear rate and shear stress were isolated by varying viscosity with dextran-supplemented medium (0–4%). **a** Melanoma migration varies under constant shear stress but increasing shear rate. **b**, **c** Constant shear rate data; migration is unchanged over an order of magnitude of shear stress. All *error bars* are mean ± SEM for $N \geq 3$

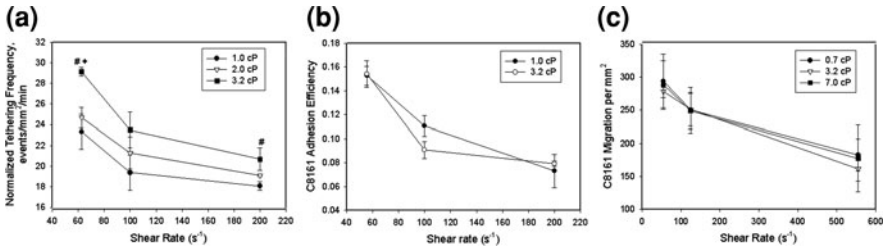

Fig. 4 Effects of shear stress on PMN tethering frequency, melanoma adhesion efficiency and extravasation at fixed shear rates. **a**, **b** fMLP-stimulated PMNs (1×10^6 cells/ml) were perfused into a parallel-plate chamber together with tumor cells (1×10^6 cells/ml). **c** Extravasation of C8161 melanoma cells with PMNs at 3 shear rates with 3 different viscosity media. All *error bars* are mean ± SEM for $N \geq 3$ and tethering data were corrected for cell flux as described by Liang et al. [53]. "**#**" indicates $P > 0.05$ as compared to 1.0 cP case and "**+**" indicates $P > 0.05$ as compared to 2.0 cP case

4.3 Relative Role of LFA-1/Mac-1 and ICAM-1 in PMN-mediated Melanoma Adhesion Efficiency

Function-blocking mAbs against CD11a and CD11b were used to elucidate how melanoma–PMN aggregates were arrested on the EC under shear conditions [53]. Blocking CD11a or CD11b, respectively, inhibited PMN-facilitated melanoma adhesion efficiency partially under all shear conditions tested (Fig. 5a). Results indicate that both LFA-1 and Mac-1 are required for melanoma cells to be maintained on the EI via aggregation to PMNs, but may have different roles. For example, blocking CD11b did not significantly alter the rate of aggregation between entering WM9 cells and tethered PMNs, and LFA-1 alone supported WM9 aggregation with tethered PMNs on the EI initially (Fig. 5b). However, after a period of 3 min, disaggregation of WM9–PMN aggregates on the EI surface proceeded more rapidly in the presence of anti-CD11b mAb than in the control. In comparison, Mac-1-dependent contact with the EI (in the presence of anti-CD11a) proceeded more slowly and reached a maximum which was approximately 25% of the control case. These aggregates remained stably adhered to the EI surface over 5 min (Fig. 5b). These results suggest that LFA-1 alone is necessary and sufficient for the initial formation of melanoma–PMN aggregates, and plays a primary role in the recruitment of melanoma cells to the EC. Mac-1 maintains the stability of melanoma arrest on the EI via the melanoma–PMN aggregation after the initial capture by PMNs.

Blocking ICAM-1 on WM9 (disrupting melanoma adhesion to PMNs) significantly reduced melanoma adhesion efficiency to the monolayer similarly to the cases of blocking E-seletin or ICAM-1 on the EI cells, suggesting that EC activation for PMN tethering is necessary in mediating melanoma cell arrest within the microcirculation.

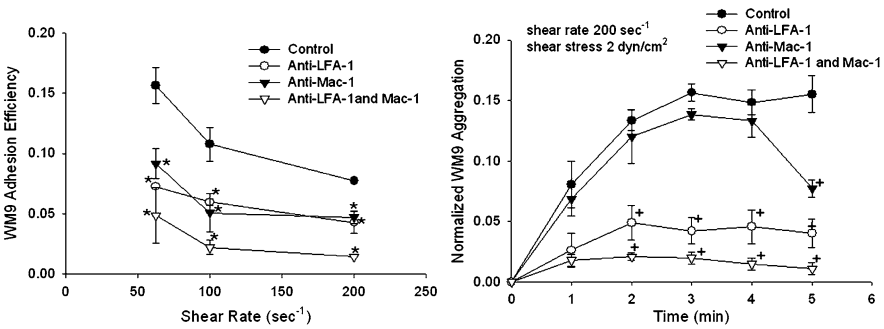

Fig. 5 Contributions of LFA-1 and Mac-1 to WM9 arrest to the EI substrate as a result of WM9-PMN collisions. **a** WM9 adhesion efficiency at different shear rates over a period of 5 min. Shear stress was 2 dyn/cm^2 for the data shown. **b** Normalized WM9 aggregation during each time course in the entire parallel-plate flow assay. $^*P < 0.05$ compared with control at the same shear rate. $^+P < 0.05$ compared with control at the same time point. Values are mean ± SEM for $N \geq 3$

4.4 Melanomas Increase Endogenous Production of IL-8 in PMNs

We first used a commercial cytokine blot (Raybiotech) to screen cytokines/chemokines in PMN–melanoma cell co-culture media. Melanoma cells and PMNs (cell # ratio was 1:1) were co-cultured in contact with each other for 6 h as described [86]. The blot detects for 42 separate cytokines in the layout shown in Fig. 6. Our first set of experiments examined those soluble factors that were secreted from C8161–PMN or WM9–PMN co-culture. In particular, we found: IL-1β, IL-6, IL-8, MCP-1 and GRO.

ELISA was subsequently used to determine the relationship between tumor metastatic potential and cytokine expressions in melanoma–PMN co-culture. Four human melanoma cell lines 1205Lu, WM9, C8161 and WM35 (ranged from high to low in metastatic potential; [74], were examined for cytokine and chemokine induction in melanoma–PMN co-cultures. PMNs co-cultured either in a Transwell (non-contact) or in contact with C8161, WM9, 1205Lu increased IL-8 expression above summed background levels from individual cell-type culture, but there was no change in IL-8 following co-culture with WM35 (Fig. 7a). In addition, co-culture of 1205Lu or WM9 with PMNs induced IL-8 production in a time-dependent manner (Fig. 7b). In contrast, the IL-8 production from WM35–PMN co-culture did not change over time. The induction of IL-8 was comparable whether cells were cultured in direct-contact or separated in a Transwell culture system indicating that *soluble signaling factorsare actively involved*. In further experiments to identify which cell type contributed to the increased amount of IL-8 in PMN–melanoma co-cultures, cell lysates were prepared from PMNs and melanoma cells following Transwell co-culture, and levels of IL-8 were detected

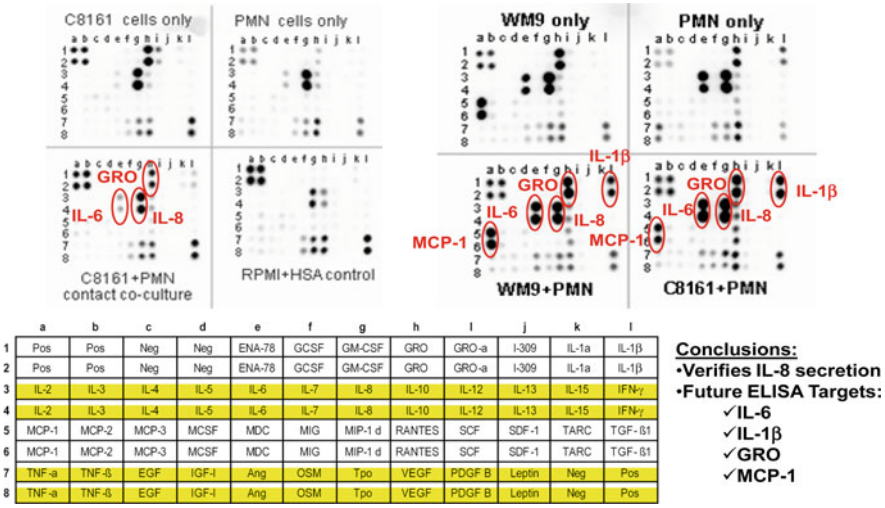

	a	b	c	d	e	f	g	h	i	j	k	l
1	Pos	Pos	Neg	Neg	ENA-78	GCSF	GM-CSF	GRO	GRO-a	I-309	IL-1a	IL-1β
2	Pos	Pos	Neg	Neg	ENA-78	GCSF	GM-CSF	GRO	GRO-a	I-309	IL-1a	IL-1β
3	IL-2	IL-3	IL-4	IL-5	IL-6	IL-7	IL-8	IL-10	IL-12	IL-13	IL-15	IFN-γ
4	IL-2	IL-3	IL-4	IL-5	IL-6	IL-7	IL-8	IL-10	IL-12	IL-13	IL-15	IFN-γ
5	MCP-1	MCP-2	MCP-3	MCSF	MDC	MIG	MIP-1 d	RANTES	SCF	SDF-1	TARC	TGF-ß1
6	MCP-1	MCP-2	MCP-3	MCSF	MDC	MIG	MIP-1 d	RANTES	SCF	SDF-1	TARC	TGF-ß1
7	TNF-a	TNF-ß	EGF	IGF-I	Ang	OSM	Tpo	VEGF	PDGF B	Leptin	Neg	Pos
8	TNF-a	TNF-ß	EGF	IGF-I	Ang	OSM	Tpo	VEGF	PDGF B	Leptin	Neg	Pos

Fig. 6 Raybiotech cytokine blot from respective C8161 and WM9 co-culture with the PMNs found IL-1β, IL-6, GRO, and MCP-1. The sensitivity for Raybiotech was at 1 pg/ml

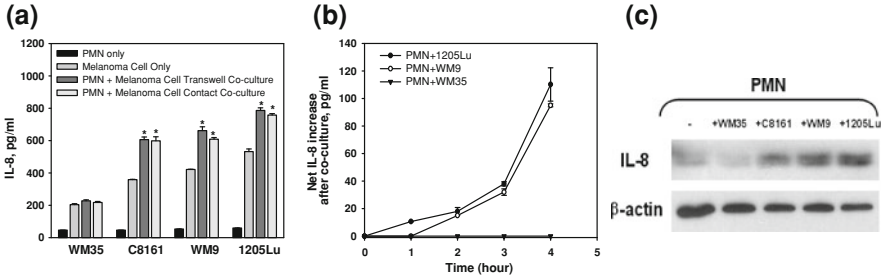

Fig. 7 Co-culturing PMNs with melanoma cells induces IL-8 increase. **a** Induction of IL-8 in PMN–melanoma cell (1205Lu, WM9 and C8161) co-cultures (contact or Transwell). $*P < 0.05$ compared with the sum of IL-8 expression from the PMN and melanoma only. **b** IL-8 increased after PMN co-culturing with 1205Lu and WM9 in a time-dependent manner. Co-culturing PMNs with WM35 did not increase IL-8 secretion over time. Values are mean ± SEM for $N \geq 6$. **c** Melanoma cells induce IL-8 production in PMNs. PMN lysates were analyzed by Western blotting with mAb against IL-8. The same blot was stripped and re-probed with mAb to β-actin. C8161, WM9 and 1205Lu induced IL-8 production in PMNs, whereas WM35 did not. Results are representative of three experiments

by Western blotting [74]. As shown in Fig. 7c, melanoma cells with higher metastatic potentials (1205Lu, WM9 and C8161) induced higher IL-8 production in PMNs, while WM35 did not induce IL-8 protein in PMNs. In contrast, IL-8 expression in melanoma cells *did not* significantly change when co-cultured in the presence or absence of PMNs [21].

4.5 Endogenous IL-8 Influence PMN Recruitment in Melanoma Cells

To characterize immunoediting of PMN activation, especially via the endogenous IL-8 chemokine within the PMN–melanoma microenvironment, Mac-1 expression on PMNs co-cultured with C8161 cells was examined using flow cytometry. Untreated PMNs and PMNs treated with blocking antibodies for IL-8 receptors CXCR1/2 were co-cultured with C8161 cells either in contact or separated by a Transwell insert [87]. Figure 8a indicates that non-CXCR1/2-blocked PMNs co-cultured with C8161 cells experienced a nearly four-fold increase in Mac-1 expression levels over those cultured alone for 4 h. The increase in Mac-1 was apparent after only 30 min of co-culture and became significant after 2 h of co-culture (data not shown). PMNs with antibody blocked CXCR1/2 showed no change in Mac-1 levels after co-cultured with C8161 cells compared with PMNs cultured alone (Fig. 8a). To understand the possibility that secreted soluble factors could be an immuno-stimulus responsible for melanoma–PMN communication, receptors CXCR1/2 on PMNs were functionally blocked. C8161 cell extravasation (assayed by the flow-migration chamber) dramatically decreased at a shear rate of 55.5 s^{-1} in the presence of CXCR1/2-blocked PMNs compared with unblocked PMNs (39% decrease), or additional IL-8-activated PMNs (73% decrease) as shown in Fig. 8b. Such effects on C8161 cell extravasation will be amplified under higher shear-rate conditions. Neutralizing anti-IL-8 mAb (1 μg/ml) was also used to bind soluble IL-8, induced or liberated by the melanoma cells, which showed similar inhibitory effects on melanoma migration as those CXCR1/2-receptor blocked PMN cases (Fig. 8b).

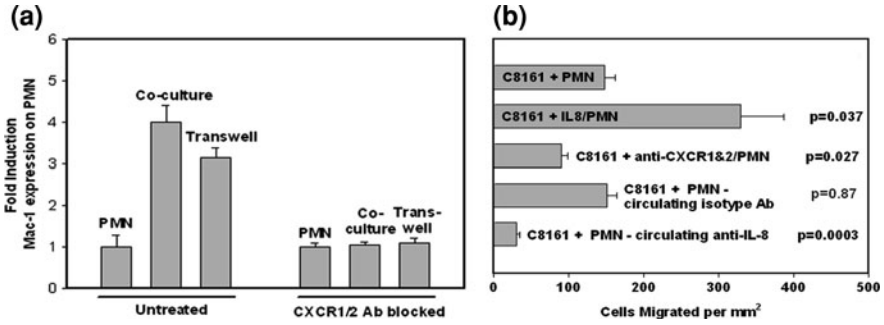

Fig. 8 Melanoma cell extravasation under flow conditions is modulated by endogenous IL-8. **a** Fold induction of Mac-1 on PMNs after co-culture with C8161. Blocking the IL-8 receptors on PMNs resulted in no increase in Mac-1. **b** Effects of IL-8 on melanoma migration mediated by PMNs. Isotype control found statistically the same as the case of "C8161 + PMN". All co-cultures were in 4 h, and all flow shear stresses were 0.4 dyn/cm^2

4.6 IL-1β and IL-6 Synergistically, but not Individually, Stimulate IL-8 Production in PMNs

After 4-6 h of co-culture, ELISAs were preformed to measure GRO-α, IL-1β, IL-6 and MCP-1 from supernatants obtained from cultures of individual cell types (e.g., PMNs only or melanomas only) or PMN–melanoma co-cultures. For all 4 melanoma cell lines tested, co-culture of PMNs with highly metastatic 1205Lu cells significantly induced IL-6 above the summed IL-6 from separate cultures (data not shown). IL-1β was produced by PMNs or melanoma cells cultured alone. It was increased after C8161, WM9 and 1205Lu were co-cultured with PMNs, albeit at a small amount (<10 pg/ml). In addition, GRO-α and MCP-1 were constitutively expressed by melanomas and co-culturing with PMNs did not change their production levels.

To investigate potential effects of different soluble factors induced or liberated by melanoma cells on IL-8 production in PMNs, human recombinant proteins including GRO-α, IL-6, and IL-1β were used to stimulate PMNs [74]. ELISA results indicated that none of these cytokines or chemokines alone was sufficient to induce IL-8 production compared with untreated PMNs (Fig. 9); however, stimulating cells with the combination of IL-1β and IL-6 increased IL-8 production in PMNs. We further confirmed the combinatorial role of IL-1β and IL-6 in melanoma-induced IL-8 induction by showing that IL-8 was significantly reduced from 781 ± 6.3 pg/ml to 680 ± 10.1 pg/ml ($P < 0.05$) in 1205Lu melanoma–PMN co-culture in the presence of neutralizing antibody against IL-1β and IL-6 (only together; not individually), indicating that IL-1β and IL-6 provide a *synergistic activation* of IL-8 in PMNs in response to melanomas.

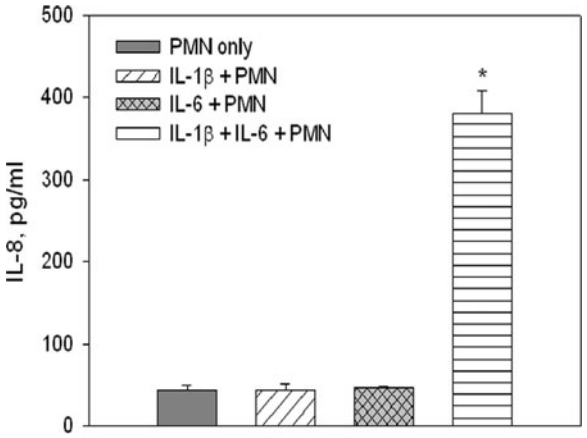

Fig. 9 IL-1β and IL-6 synergistically increased IL-8 production in PMNs compared with untreated PMNs. *$P < 0.05$ compared with other three cases. Values are mean ± SEM for $N > 3$

4.7 Fluid Convection Affects IL-8-mediated PMN Activation Within the Tumor Microenvironment

To investigate how the fluid convection affects IL-8 signaling by melanoma cells, which in turn affects the expression of LFA-1 and Mac-1 on PMNs and modifies tumor cell adhesion to the EC, Comsol Multiphysics was used to simulate the convection and diffusion of IL-8 from a moving cell under flow conditions (Fig. 10). To simulate the system, a tumor cell was assumed to be in the free stream in the near-wall region and its velocity was derived based on the shear flow condition, using Eq. 3. A PMN was assumed to roll on the EC at the experimentally derived average rolling velocity for the shear condition. The local IL-8 concentration near a rolling PMN and the time at which the PMN is activated by the transported IL-8 were derived to determine the extent of LFA-1 and Mac-1 activation.

Results indicate that altering the shear rate affects the IL-8 concentration near a rolling PMN at different time points (Fig. 11). When the shear rate was constant at 62.5 s^{-1}, the IL-8 concentration near a rolling PMN and the stimulation time remained constant under various shear stresses (Fig. 11a). In contrast, when the shear stress was constant at 2 dyn/cm^2 and shear rate increased from 62.5 to 200 s^{-1}, it took less time to activate the PMNs under a higher shear rate (Fig. 11b). These data suggest that the fluid convection affects the local concentration of IL-8 near a downstream PMN as well as the time needed to activate the PMN, which is important in up-regulating the expression of LFA-1 and Mac-1.

The changes of LFA-1 and Mac-1 site densities on a rolling PMN upon stimulation from IL-8 secreted by a tumor cell in a shear flow were then calculated based on the flow cytometry measurements on LFA-1/Mac-1 expressions on

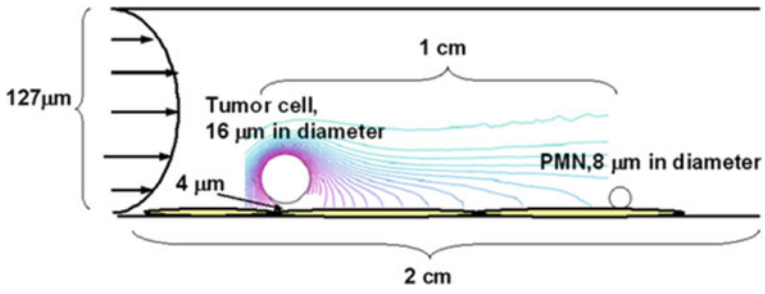

Fig. 10 A parallel plate is 2 cm in length and 127 μm in height. IL-8 was assumed to be constitutively secreted from a moving tumor cell and evenly distributed on cell surface. The concentration of IL-8 secreted by one tumor cell was determined by ELISA as described in Sect. 2. The tumor cell was assumed to travel in a shear flow near the EC substrate; while a PMN was assumed to be rolling on the EC in the downstream. Simulation started when a tumor cell and a PMN were 1 cm apart. The concentration of IL-8 secreted by the moving tumor cell near the rolling PMN was derived by using Comsol Multiphysics simulation under various shear flow conditions

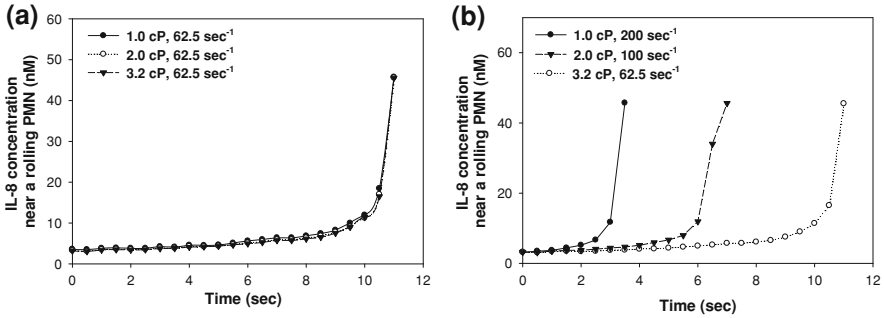

Fig. 11 The concentration of IL-8 near PMN and the time it activates PMN under different shear flow conditions. Comsol Multiphysics was used to simulate the diffusion of IL-8 as described in Sect. 2, and then the concentration of IL-8 near the PMN was derived. The activation time of IL-8 on the PMN was determined by the duration melanoma cell used to reach the PMN. **a** IL-8 concentration near a rolling PMN and the time it activated the PMN was about the same under same shear rate but different shear stresses, **b** the higher shear rate let tumor cell travel faster towards PMN, resulting in shorter period of stimulation on PMN under same shear stress but different shear rates

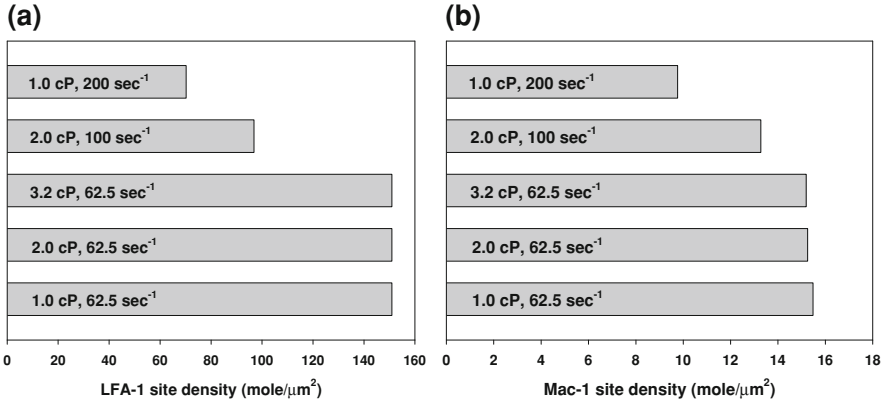

Fig. 12 LFA-1 and Mac-1 expressions upon activation of IL-8 from tumor cell under different shear flow conditions. LFA-1 and Mac-1 site densities on the PMN under various shear conditions were derived using the site density expression data [51] and the simulation data shown in Fig. 11. **a** Mac-1 expression, **b** LFA-1 expression. At the same shear rate, LFA-1 and Mac-1 expressions on PMN did not have much difference although the shear stresses were different. In contrast, when the shear stress is the same, the increase of shear rates reduced LFA-1 and Mac-1 expressions

PMNs stimulated by dose-dependent IL-8 (Fig. 12). Results indicate that at a constant shear rate, 62.5 s^{-1}, varying the shear stress does not alter the expressions of LFA-1 and Mac-1 on PMNs. However, at a constant shear stress, 2 dyn/cm^2, LFA-1 and Mac-1 expressions on PMNs were reduced when shear rate is increased.

4.8 Melanoma–PMN Binding Association Rate is Affected by the Shear Rate

To quantify the increase in binding potential when a PMN is stimulated by IL-8 secreted from a melanoma cell, the association rate governing the binding of the cells was calculated. The likelihood of binding between the two cells is determined by the number and availability of adhesion molecules on both cells, as well as the intrinsic binding properties of the molecules. Equation 6 was used to calculate the association rate for an LFA-1 and a Mac-1 molecule binding with an ICAM-1 molecule when a melanoma cell is 1 μm from a rolling PMN under various shear conditions. The surface densities of LFA-1 and Mac-1 molecules on a PMN stimulated by melanoma cell-derived IL-8 (Fig. 12) were used for n_L (Eq. 6). A constant separation distance and contact area were assumed for the six shear flow conditions.

The association rates indicate that the likelihood of an LFA-1/ICAM-1 bond forming between a melanoma cell and PMN is almost doubled when the shear rate is decreased from 200 to 62.5 s^{-1} and the shear stress is considered constant (Fig. 13). For Mac-1/ICAM-1 binding, the likelihood increases by more than twice when the shear rate is decreased. When the shear rate remains constant, however, and the shear stress is increased, the binding potential for both molecules remains constant [51].

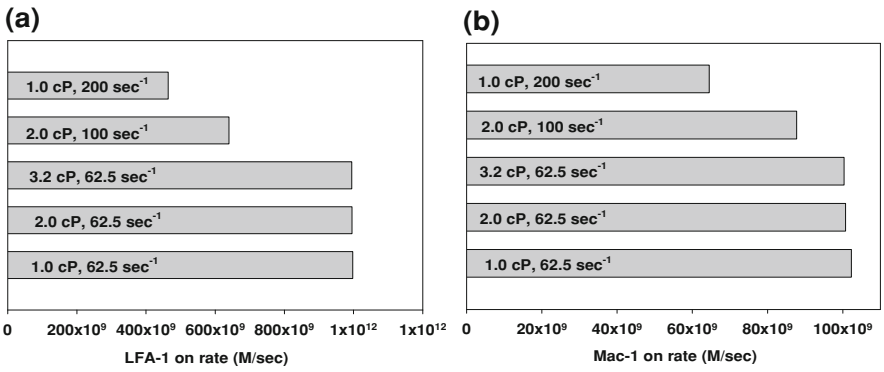

Fig. 13 Association-rate for LFA-1 and Mac-1 binding to ICAM-1 upon stimulation from IL-8 under different shear flow conditions. Association-rates for LFA-1 and Mac-1 binding to ICAM-1 when the molecules are up-regulated due to IL-8 stimulation from an upstream melanoma cell. **a** LFA-1/ICAM-1 binding association-rate, **b** Mac-1/ICAM-1 binding association-rate. Both the LFA-1/ICAM-1 and Mac-1/ICAM-1 association-rates are dependent on the shear rate and not the shear stress of the flow

4.9 Bond Force Between Melanoma Cell and PMN Under Different Shear Conditions

The dissociation of β_2 integrin bonds with ICAM-1 is governed by the force applied to them. In order to compare the effect the shear rate and shear stress have on the bond dissociation, a single bond was examined under various flow conditions. A numerical model was used to simulate a melanoma cell and a stationary PMN to determine the peak force applied to the melanoma cell due to a single bond between the cells under various shear conditions [34, 51]. In all simulations, the melanoma cell was initially located above and slightly downstream of the stationary PMN (Fig. 14) and then was allowed to move freely at its steady state velocity for each flow condition. The melanoma cell was acted upon by the fluid, bond, and repulsion forces until a maximum bond force was reached. Although adhesion between a melanoma cell and a PMN may be mediated by more than a single bond, the trend in bond dissociation over various flow conditions is expected to be similar for all bonds.

Results indicate that increasing the shear rate from 62.5 to 200 s^{-1}, while maintaining a constant shear stress, increased the maximum bond force by approximately 11%, but increased the rate at which it was reached by almost four times (Fig. 15). Increasing the shear stress from 0.625 to 2 dyn/cm^2, while keeping a constant shear rate, increased the maximum bond force by almost twice, and decreased the rate which it was reached by almost five times. Together, these results suggest that the dissociation of bonds between the melanoma cell and PMN is governed by both the shear stress and the shear rate.

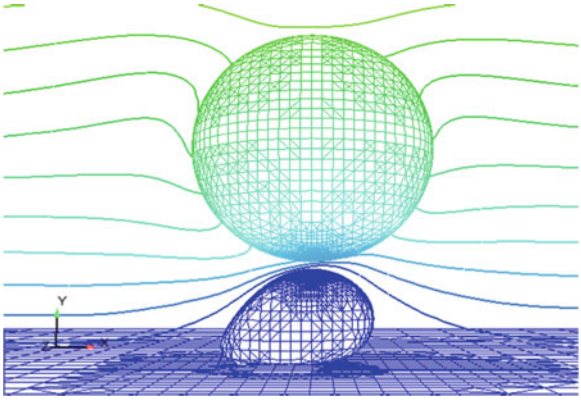

Fig. 14 Melanoma cell bound to a stationary PMN via a single bond. Initial configuration of the cells, with a line between them to represent the location of the bond

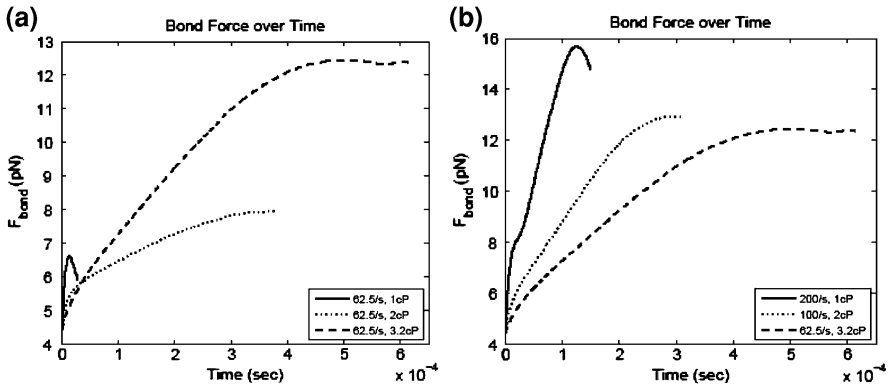

Fig. 15 Force on a melanoma cell due to a single bond with a stationary PMN under various shear conditions. Melanoma cell motion was simulated numerically due to the action of a single bond with a PMN. **a** Under the same shear rate, at higher shear stress (due to higher viscosity), the bond force peaks slower, but at a greater force than at lower shear stress, **b** Under the same shear stress, at a higher shear rate, the bond force reaches a maximum faster and at a greater force than at lower shear rates. These results indicate the maximum force applied to the melanoma cell due to the bond and the time it takes to reach it is dependent on both shear rate and shear stress

4.10 Melanoma Interactions with the Endothelial Cells

Melanoma cells induce VE-cadherin junction disassembly through tumor-secreted soluble proteins and endothelial VCAM-1 receptor-mediated events. Fluorescence imaging of HUVECs stained for VE-cadherin showed disruption of VE-cadherin junctions when co-cultured with A2058 melanoma cells over time (Fig. 16). Compared to intact VE-cadherin junctions in the case of HUVECs cultured in control medium (Fig. 16a), the breakdown of VE-cadherin was evident through the discontinuity of the green fluorescent line labeling the VE-cadherin junctions (gaps at 45 min are shown in Fig. 16b). The corresponding bright field images (Fig. 16c) show that the A2058 melanoma cells were located within the sites of gap formation. These results show that highly metastatic melanoma cells induce breakdown of VE-cadherin junctions.

Disruption of VE-cadherin was identified from analysis of discontinuity of green fluorescence at VE-cadherin junctions between HUVECs. Gap area within disrupted VE-cadherin junctions was determined from six images (see asterisks in Fig. 16b as an example). Gap area was quantified as the ratio of pixels within all the gaps and the total number of pixels in one image [39]. The average% endothelial gaps was calculated from six images and plotted as a function of time (Fig. 16d).

To determine if VE-cadherin disassembly was primarily mediated by soluble factor or receptor/ligand binding signals, HUVECs were brought in contact with tumor conditioned medium (TCM) or melanoma cells with increasing metastatic potential for 45 min. Melanoma cells with increased metastatic potential, or TCM

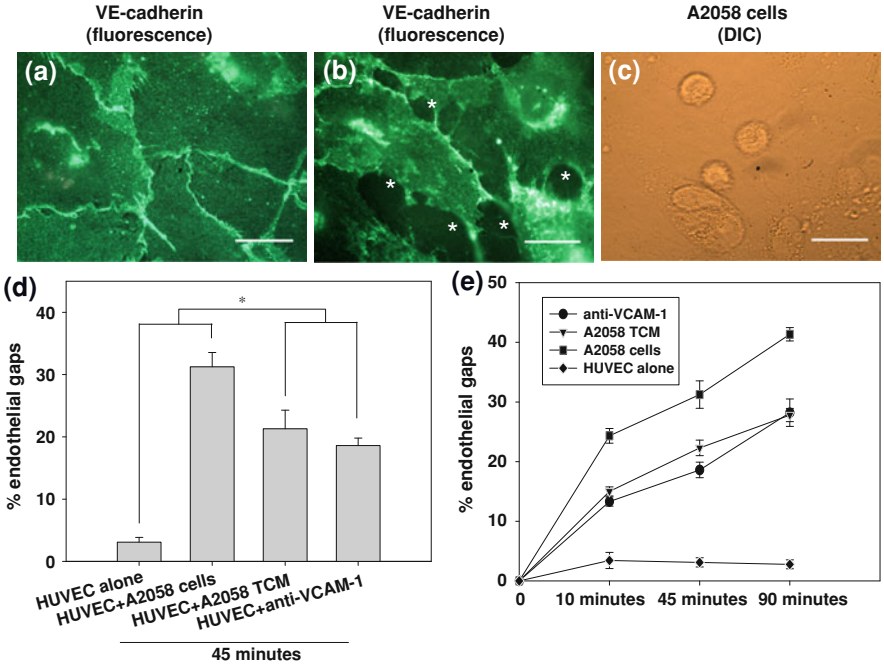

Fig. 16 Melanoma cells induce VE-cadherin disassembly. *Bars* 5 μm (**a**–**h**). **a** VE-cadherin junctions in HUVECs without A2058 melanoma cells. HUVECs were fixed, permeabilized, and stained with anti-VE-cadherin mAb followed by Alexa 488. Representative fields were examined and show intact VE-cadherin junctions indicated by intact *green fluorescent borders*. **b** Disruption of VE-cadherin junctions after HUVECs were in direct contact with A2058 tumor cells for either 10, 45, or 90 min (45 min is shown) using FITC. **c** The same field of view captured under bright field, shows tumor cells in regions coinciding with gap formation. *Asterisks* show disruption of VE-cadherin homodimers. **d** HUVECs co-cultured with TCM or anti-VCAM-1 significantly increase % gap formation compared to HUVECs alone, but less gap formation than A2058 cells co-cultured with HUVECs. *P* values are comparing % endothelial gap of HUVEC + TCM and HUVEC + anti-VCAM-1 with % endothelial gap of HUVEC alone and HUVEC + A2058 cells ($^*P < 0.05$). For all experiments, values are mean ± SD. **e** The % endothelial gaps as a function of time are plotted. Experiments show the % endothelial gaps over time when A2058 TCM, anti-VCAM-1, or A2058 cells are co-cultured with HUVECs over 10, 45, or 90 min

from those cells showed a significant increase in ability to induce gap formation, indicating an increase in VE-cadherin disassembly (Fig. 16d). Also, HUVECs stimulated with anti-VCAM-1 showed a significant increase in gap formation (Fig. 16d) similar to that seen in the presence of TCM. However neither anti-VCAM-1 nor TCM induced the same degree of endothelial gaps as A2058 cells in co-culture with HUVECs (Fig. 16d).

Since both anti-VCAM-1 and TCM induced a gradual increase in the percentage endothelial gap formation over time (Fig. 16e), Khanna et al. [39] further found that VCAM-1 induces a transient VE-cadherin disassembly, while soluble

proteins show a prolonged effect thus enlarging existing gaps to allow the passage of melanoma cells, where the number of gaps after 90 min.

4.11 Secretion of IL-8 and IL-1β by Melanoma Regulates VE-cadherin Junction Disassembly

Cytokines present within TCM secreted by melanoma cells over 24 h were analyzed using a Raybiotech cytokine blot. We found that several cytokines were secreted by melanoma cell types at high concentrations including IL-8, IL-6, IL-1β, and GRO-α [39]. These cytokines were further quantified using ELISA. Clearly, highly metastatic melanoma cells (e.g., 1205Lu) produce higher concentrations of these soluble cytokines compared with those of lesser metastatic potential (e.g., WM35). Stimulating HUVECs with recombinant forms of individual cytokines (at the same concentrations as that in A2058 TCM) showed little increase in the percentage of gap area (Fig. 17a). Combining cytokines in TCM, specifically IL-8 and IL-1β only had additive effects on VE-cadherin disassembly rather than being synergistic (Fig. 17b, c).

Since concentrations of cytokines in TCM are simply the bulk concentrations, HUVECs in direct contact with melanoma cells may sense much higher local concentrations of cytokines within the cell–cell contact region than that found in TCM. We therefore specifically addressed whether IL-8 or IL-1β is involved in this response by neutralizing these cytokines secreted from melanoma cells that are in contact with HUVECs. Neutralization of either IL-8 or IL-1β decreased VE-cadherin disassembly; however, the endothelial gaps were still comparable to that induced by anti-VCAM-1 and there are still more gaps compared to HUVECs alone (Fig. 17d). However, simultaneous neutralization of IL-8 and IL-1β reduced the breakdown of VE-cadherin junctions (Fig. 17e). These results show the importance of these cytokines in melanoma induced VE-cadherin disassembly in the presence of VCAM-1 interactions. Furthermore, using neutralization antibodies we confirmed that IL-8 and IL-1β both play significant roles in the breakdown of VE-cadherin junctions.

Recent studies by Khanna et al. [39] has further found that melanoma signals via TCM soluble proteins and VCAM-1-mediated receptor induce phosphorylation of p38 MAP kinase that regulates VE-cadherin disassembly. The functional role of p38 in endothelial cells during melanoma extravasation has also been examined using small interfering RNA (siRNA) approaches. siRNA mediated knockdown of p38 (and thus p-p38) in HUVECs was confirmed using western blotting. When p38 expression was knocked down, melanoma extravasation through the endothelial barrier (after 4 h) decreased to nearly 40% compared to the control [39]. These results show that p38 is not only important in the regulation of VE-cadherin junctions, but also in overall tumor extravasation.

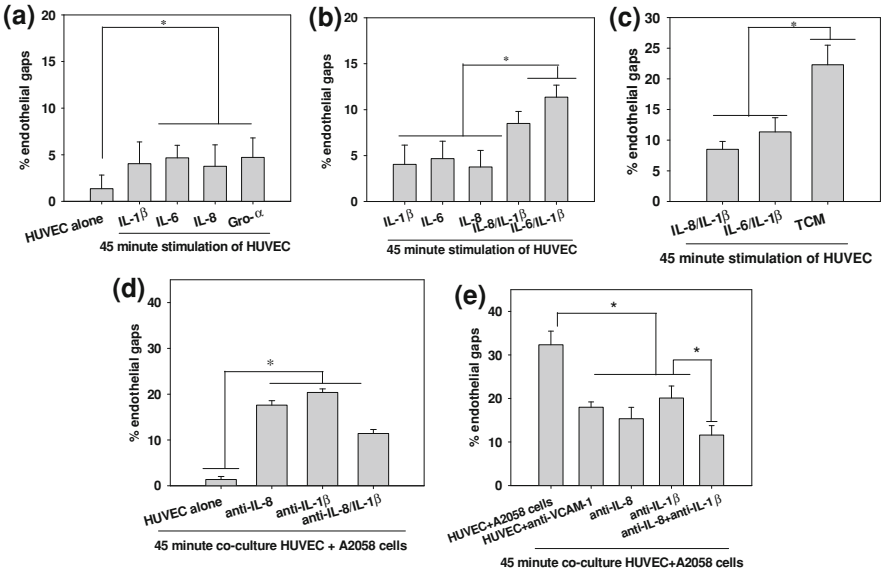

Fig. 17 **a–c** IL-8 and IL-1β have additive rather than synergistic effects on VE-cadherin disassembly: **a** the indicated cytokines induced VE-cadherin disassembly. *P* values are comparing % gap induced by cytokines with % gap of HUVEC alone ($^*P < 0.05$). **b** Stimulation of HUVECs with recombinant combined forms of IL-8/IL-1β or IL-6/IL-1β induced additive effects on endothelial gap formation compared with individual forms. Concentrations of cytokines were based on TCM concentrations measured using ELISA [39]. *P* values ($^*P < 0.05$) compare % gap area of combinations of cytokines with % gap of HUVEC + IL-8, HUVEC + IL-6, HUVEC + IL-1β. **c** Combinations of cytokines induced significantly less gap formation than TCM alone. *P* values are comparing % gap area of TCM with % gap of HUVEC + IL-8/IL-1β, HUVEC + IL-6/IL-1β. **d–e** Anti-VCAM-1 and neutralization of both IL-8 and IL-1β dramatically reduces the breakdown of VE-cadherin: **d** HUVECs were contacted with A2058 cells + anti-IL-8, A2058 cells + anti-IL-1β, or A2058 cells + anti-IL-8 + anti-IL-1β. *P* values are comparing each experimental condition with % endothelial gap areas during HUVEC alone ($^*P < 0.05$). **e** Using the same controls as in panel **d**, data was graphed to make comparisons between the effects of neutralizing individual and pairs of cytokines. HUVECs were contacted with either A2058 cells, A2058 cells + anti-VCAM-1, A2058 cells + anti-IL-8, A2058 cells + anti-IL-1β, or A2058 cells + anti-IL-8 + anti-IL-1β. Neutralization of both IL-8 and IL-1β dramatically decreased % endothelial gaps compared to HUVECs stimulated with anti-VCAM-1 or anti-IL-8 and anti-IL-1β alone. *P* values are comparing each experimental condition with % endothelial gap areas for HUVEC + anti-VCAM-1, HUVEC + A2058 cells + anti-IL-8, and HUVEC + A2058 cells + anti-IL-1β ($^*P < 0.05$). Values for graphs are mean ± SD

4.12 Transient Melanoma Cells in Lungs Secrete IL-8 to Attract PMNs Thereby Promoting Retention in vivo

To demonstrate that transient metastatic melanoma cells in lungs secrete IL-8, which recruited PMNs resulting in cellular interactions promoting melanoma cell retention, GFP-tagged 1205Lu human melanoma cells nucleofected with siRNA targeting IL-8 were injected into the lateral tail vein of nude mice. One hour later

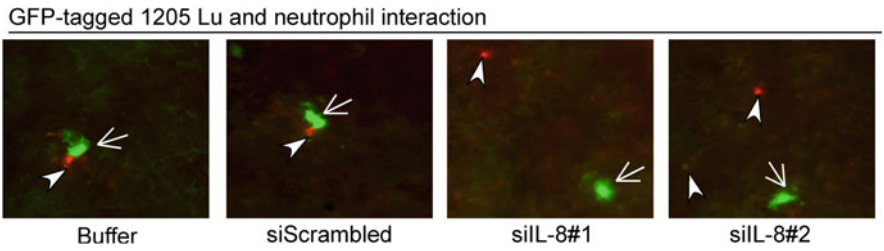

Fig. 18 Decreasing IL-8 secretion from melanoma cells reduced interaction with exogenously added human PMNs in lungs. Co-localized PMNs (*red; arrow heads*) and melanoma cells (*green; arrows*) were more abundant in controls compared to melanoma cells having reduced IL-8 secretion (siIL-8#1&2; 100×)

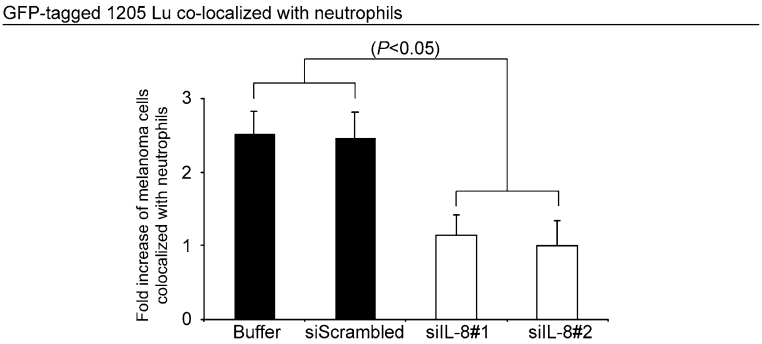

Fig. 19 Decreased IL-8 secretion from melanoma cells, reduced human PMN co-localization with melanoma cells in the lungs of nude mice. All data are mean ± SEM, representing at least 2 independent experiments

human CellTracker Orange CMTMR stained human PMNs were injected in the opposite tail vein. Twenty-four hours later, co-localized green melanoma cells and red PMNs were photographed and quantified (Fig. 18).

Decreasing IL-8 expression in melanoma cells (cases in siIL-8#1 and siIL-8#2) reduced co-localization with PMNs by ~60% compared to buffer and scrambled siRNA controls (Fig. 19). Thus, transient melanoma cells secrete IL-8 to attract PMNs, which then interact with the melanoma cells promoting shear-resistant tethering retention within the lung circulation to enhance the possibility of extravasation under flow conditions and subsequent metastasis development.

4.13 Decreasing Secreted IL-8 from Metastatic Melanoma Cells Reduced in vivo Lung Metastasis Development

While decreasing IL-8 secreted from melanoma cells led to less interaction with PMNs and retention of fewer cells in lungs, it was uncertain whether retained cells

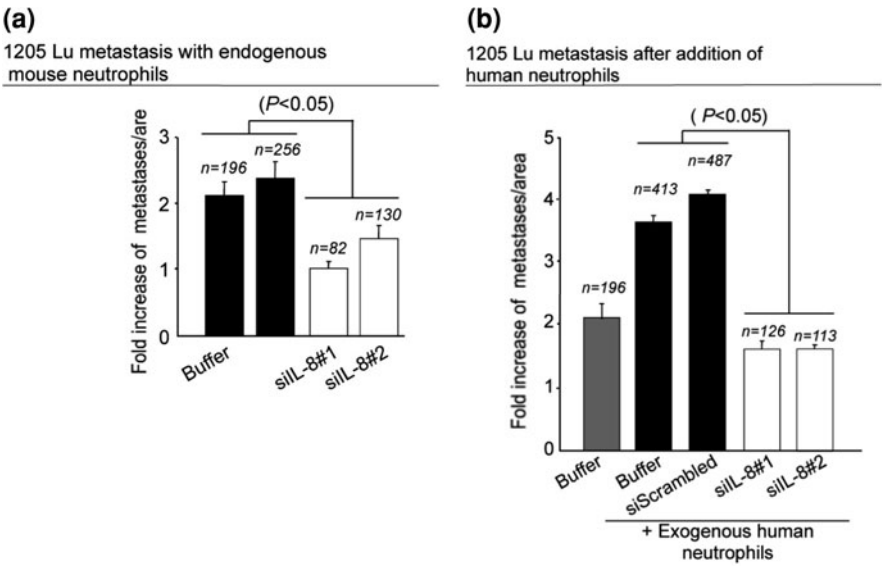

Fig. 20 Decreasing IL-8 expression in melanoma cells reduced lung metastases formation. SiRNA-mediated targeting of IL-8 in melanoma cells, decreased development of GFP-tagged 1205Lu lung metastasis development in the presence of **a** endogenous mouse PMNs; and **b** exogenous human PMNs. Human PMNs doubled rate at which melanoma lung metastases developed. Decreasing IL-8 secretion from melanoma cells reduced lung metastasis formation to control levels. All data are mean ± SEM, representing at least 2 independent experiments

would develop into more lung metastases. Therefore, siRNA was used to decrease IL-8 protein levels in GFP-tagged 1205Lu cells that were injected into the tail vein of nude mice with only the endogenous mouse PMNs present. Total number of metastatic nodules in the lungs was quantified by fluorescence microscopy 18 days later. Reducing IL-8 expression in and secretion from melanoma cells, decreased number of metastases by 50–60% for 1205Lu (Fig. 20a). Similar results were observed for C8161.Cl9 cells (data not shown).

To show that PMNs in the mouse bloodstream directly interact with transient IL-8 secreting melanoma cells, GFP-tagged 1205Lu cells having endogenous or reduced IL-8 expression were injected into the lateral tail vein of a nude mouse. One hour later, human CellTracker Orange CMTMR stained human PMNs were injected in the opposite tail vein. Total number of metastatic nodules in the lungs was quantified by fluorescence microscopy 18 days later. Addition of human PMNs doubled the number of metastases developing in the lungs of mice compared to that observed with just endogenous mouse PMNs and siRNA-mediated targeting of IL-8 reduced interaction to that observed in control cells (Fig. 20b; scale set to that in Fig. 20a). Thus, decreasing IL-8 levels secreted by melanoma cells reduced interaction with PMNs, which led to the development of fewer lung metastases.

5 Discussions

It is well reported in the literature that tumor cells do not use the same processes that have been described for leukocyte adhesion and migration through an endothelial barrier. While not true of all tumor cells, melanoma cells characterized as highly metastatic, express neither ligands for endothelial selectin molecules nor β_2 integrins at a level necessary to maintain shear-resistant adhesion to endothelial ICAM-1. It has been suggested that initial microvascular arrest of metastasizing tumor cells (from cell lines of six different histological origins) does not occur "leukocyte-like rolling" adhesive interaction with the EC [92].

Recent study showed under dynamic flow conditions, PMNs could influence melanoma cell adhesion to the EC by binding to ICAM-1 on both melanoma and ECs with their β_2 integrins thereby enhancing subsequent melanoma cell migration through the EC (Figs. 2, 5). The difference between the melanoma cell migration and the PMN tethering results under hydrodynamic forces supports the theory that PMNs facilitate TC migration. If melanoma cells used the traditional extravasation mechanism of binding to the EC itself, the response to shear would have been expected to be similar to that seen in single cell tethering (Fig. 4a). However, this is not the case. The results indicate two separate bonds are necessary for melanoma cell migration (Figs. 1a, 2) and the interesting shear-rate dependence becomes apparent (Figs. 3, 4c). The migration experiments examine adhesion of TCs to PMNs after PMNs have already adhered to the EC, whereas the tethering results more specifically focus on PMN to EC adhesion. The migration data shows TC to PMN adhesion is shear-rate dependant and parallel-plate flow chamber data of PMN to TC aggregation shows a similar trend (Fig. 4b). PMN tethering interactions, mediated by selectins, are a prerequisite for subsequent adherence, mediated by β_2 integrins on PMNs binding to ICAM-1 on the EC. Shear rate is inversely proportional to intercellular contact time. By decreasing shear rates, PMNs are in contact with the EC longer, which allows firm binding to occur. The same mechanism may be at play between PMNs and melanoma cells; a lower shear rate may increase the time the cells are in contact, therefore allowing more heterotypic binding and consequently more extravasation.

Jadhav and Konstantopoulos [38] have shown that ICAM-1-expressing colon carcinoma cells (HCT-8) bind to PMN under shear as a function of both contact duration and shear stress whereas sLe^x-expressing carcinoma cells (LS174T) bind to PMN as a function of only contact duration. Their experimental setup was a cone-plate viscometer where two cell types (PMN and TC) were allowed to collide and aggregate under a shear in a free suspension. Similar recent work by Liang et al. [49, 54] had shown shear-rate dependent PMN–melanoma binding under the flow using the cone-plate shear assay. In contrast, the data presented here is from a three-cell system (Fig. 1; PMN, TC and EC) where two separate binding events must occur near a planar surface. Cone-plate shear results on heterotypic cell–cell binding provided excellent insight into the kinetics of PMN–TC aggregation, but might not be expected to explain the results of PMN–TC aggregation mediated

melanoma cell adhesion to and migration through the EC presented here, due to the binding of PMN on the EC in addition to PMN–melanoma aggregation.

IL-8 plays a crucial role in regulating cell function for host defense and natural immunity [91]. IL-8 is released by various cell types, including PMNs, monocytes, T lymphocytes and ECs, upon exposure to inflammatory stimuli, such as TNF-α, IL-1 and LPS [7, 59]. IL-8, in particular, is a major mediator of PMN activation and migration. IL-8 has been previously shown to activate Mac-1 up-regulation in PMNs which facilitates melanoma cell migration under flow conditions [86]. Consistent with this observation, we have also found that IL-8 neutralization leads to a reduction in melanoma transmigration (Fig. 8).

Melanoma cells have been reported to express IL-8 and this influences their oncogenic properties [71], including their metastatic abilities. In the current study [74], we have shown that IL-8 is constitutively produced by melanoma cells regardless of their metastatic potentials (Fig. 7). Furthermore, PMNs do not influence IL-8 expression in melanoma cells. However, tumor metastatic potentials were directly related to the ability of the melanoma cells to induce IL-8 production in PMNs (Fig. 7). IL-8 has been shown to induce Mac-1 expression in PMNs; therefore, melanoma cells with high metastatic potentials (1205Lu, WM9 and C8161) directly alter the microenvironment by modifying PMN function and expression of chemokines and integrins to promote extravasation through β_2 integrin-ICAM-1 bindings under flow conditions, while there is no significant effect under static conditions.

PMN-generated CXC chemokines can act through autocrine or paracrine mechanisms to amplify PMN inflammatory activities via suppression of apoptosis [28]. In the study, paracrine mechanisms are operative since melanoma-derived IL-8 is required for induction of IL-8 in PMNs (Fig. 8). IL-8 binds with high affinity to two distinct receptors, CXCR1 and CXCR2. Blocking these two receptors on PMNs significantly reduced IL-8 induction after PMN and melanoma cells are co-cultured, but did not reduce the production of IL-8 to the summed background level of the PMN and melanoma cells indicating that there are cytokines other than IL-8, such as IL-1β and IL-6, which are responsible for the increase of IL-8 secretion after co-culture (Fig. 9).

One important mode of intercellular communication in cancer hematogenous metastasis occurs through the soluble chemokines released by involved cells, which may be affected by hydrodynamic shear flow. Melanoma cells constitutively secrete the inflammatory chemokine IL-8. When in a shear flow, this IL-8 is transported and stimulates other cells in the flow. A numerical model was employed to investigate the effects of the transported IL-8 on PMNs in a shear flow [51]. Results show that shear rate, rather than shear stress, affects the IL-8 concentration near a rolling PMN at different time points (Fig. 11). Thus, the surface density of LFA-1 and Mac-1 on the stimulated PMN is also shear rate dependent (Fig. 12). The binding potential of IL-8 stimulated PMNs (mediated by both LFA-1/ICAM-1 and Mac-1/ICAM-1 binding) followed the same shear rate dependent trend, which implies the transport of IL-8 to a rolling PMN contributes

to the shear rate dependence of melanoma cell adhesion to the EC in the presence of PMNs in a hydrodynamic shear flow.

The dissociation of melanoma cells from PMNs is determined by the force applied to the intercellular bonds. In the numerical simulations presented, the force applied to a single bond between the cells was modeled in order to directly compare the results under various flow conditions. Though cell adhesion is expected to be mediated by more than one bond, the trend of bond dissociation is expected to be similar to the trend seen in the single bond situation. Thus, we can make a general conclusion on the trend in bond dissociation between the cells based on the numerical simulations. Changing either the shear rate or the shear stress altered the trend of the force applied to the melanoma cell by a single bond. This suggests that the dissociation of the bonds between a melanoma cell and a PMN is dependent on both the shear rate and shear stress. Since the melanoma cell–PMN aggregation through β_2 integrins and ICAM-1 is affected by shear rate, but the dissociation of bonds between the cells is dependent on both the shear rate and shear stress, it is probable that the formation of bonds between the two cells plays a more important role in determining the aggregation potential than the bond dissociation (Fig. 15).

The interaction of TCs with ECs is a key step in facilitating melanoma metastasis. However, research on drug therapies to treat such cancers has focused on single cell studies without considering the effects of tumor interactions with normal cell physiology. In several studies A2058 melanoma cells were used to study VE-cadherin disassembly since they are characterized by highly invasive capabilities and secrete high levels of soluble proteins, including growth factors and moderate levels of IL-8, IL-6, IL-1β, and GRO-α, and serve as an ideal system in studying metastasis [55, 74, 93]. Melanoma cells induce an increase in endothelial gap formation with increasing tumor cell concentration. In addition, melanoma cells with higher metastatic capabilities induce larger sized gap areas that increase over time corresponding to a higher degree of VE-cadherin disassembly. Khanna et al. [39] showed that anti-VCAM-1 initially induces the breakdown of VE-cadherin gap formation, with an increase in the number of gaps with a size of 100,000 pixels or greater after 10 min (Fig. 16). However, after 45 and 90 min, there is a decrease in the number of larger gaps (>100,000 pixels), which shows that the gaps formed by anti-VCAM-1 are closing after 10 min. On the other hand, the release of soluble cytokines including IL-8 and IL-1β prolong the time over which gaps remain open, which correlates with greater VE-cadherin disassembly (Fig. 16). This phenomenon is shown by the gradual increase in the number of large gaps (size of 100,000 pixels or greater) over 90 min. The changes in the number of gaps correlate with phosphorylation of p38 MAP kinase where greater phosphorylation levels of p38 correlate with an increase in the number of gaps [39].

In vivo studies have illustrated that VE-cadherin junction breakdown is an important event during melanoma metastasis [24]. These results show that the injection of nude mice with BV13 (anti-VE-cadherin antibody, which induces VE-cadherin disassembly) results in a four-fold increase in tumor metastasis and

an increase in overall permeability of the endothelial layer. While these studies have focused on the in vivo aspects of VE-cadherin roles, our present in vitro studies provide the evidence that shows the importance of soluble cytokines released from melanoma in regulating VE-cadherin junctions. In particular, we found IL-8 and IL-1β play a prominent role in soluble factor mediated breakdown of VE-cadherin junctions (Fig. 17). These results are consistent with previous in vivo studies that show that $CXCR2^{-/-}$ nude mice injected with melanoma cells result in a decrease in melanoma metastasis [85]. In addition, soluble proteins alone are capable of facilitating the breakdown of these junctions showing that melanoma metastasis is not primarily mediated by adhesion events, but rather that both VCAM-1 and soluble proteins control the temporal disassembly of VE-cadherin.

IL-8, involved in which was originally identified as a PMN chemoattractant [71], is one of the potent inflammatory cytokines influencing melanoma development [2, 9, 83, 84]. However, the role that IL-8 plays mediating PMNs–melanoma interactions within the circulation and thereby promoting in vivo extravasation and subsequent metastasis development has remained uncertain until now.

Recent studies by Huh et al. [36] reported that targeting intracellular IL-8 in melanoma cells using siRNA reduces concentrations of secreted IL-8 in the extracellular microenvironment involving PMNs, which further decreases PMN–melanoma cell aggregations in vivo (Figs. 18, 19) as well as melanoma adhesion to the EC under the dynamic conditions of blood flow. PMN-mediated extravasation of melanoma cells was significantly reduced under flow conditions following inhibition of intracellular IL-8 from melanomas, which is an agreement with prior reports in using neutralizing soluble IL-8 directly within the circulation [21]. Mechanistically, decreasing secreted IL-8 from melanomas disrupted interactions between ICAM-1 expressed on melanoma cells and β_2 integrins, especially Mac-1 on PMNs, which reduced tethering of cells to the lung endothelium under flow conditions. Previous studies have shown that IL-8 secretion from melanoma cells induced endogenous IL-8 production from PMNs after co-culture of PMNs and melanoma cells [74], which was also observed in this study. Thus, tumor-recruited PMNs can play an important role modulating metastasis by holding transient melanoma cell in place within the circulation in the lungs for a sufficient period of time to facilitate extravasation across the endothelial lining to promote development of in vivo metastases (Fig. 20). While the importance of PMN-mediated melanoma extravasation in lung tissue is demonstrated in this report, it is speculated that this process also promotes metastasis in other organs. It is also possible that PMNs hold melanoma cells in place in the capillaries until the cells grow into a secondary tumor, which is a possibility that has not been explored in this study.

In summary, secreted IL-8 from metastatic melanoma cells do not seem to affect cellular growth or tumor development but attracted PMNs to melanoma cells. Up-regulated β_2 integrin expression on PMNs facilitates interaction with melanoma cells, which promoted shear-resistant binding between ICAM-1

expressing melanoma cells and PMNs to the EC, thereby promoting melanoma extravasation and subsequent lung metastasis development. Thus, IL-8 plays an important role in PMN-mediated melanoma cell retention in the lungs and if targeted, could have significant therapeutic potential to reduce metastasis development.

Acknowledgment The author thanks his former and current graduate students for their outstanding contributions to the work presented in this chapter, especially Dr. Margret Slattery, Dr. Shile Liang, Dr. Hsin H. Peng, Dr. Meghan Hoskins, Ms. Payal Khanna and Ms. Tara Yunkunis. He greatly acknowledges Dr. Gavin Robertson, Dr. Arati Sharma, Dr. Avery August, and Dr. Robert Kunz (all from Penn State University), who have contributed significant collaboration to the work. Gratitude also extends to Dr. Meenhard Herlyn (Wistar Institute, Philadelphia, PA, USA), Dr. Danny Welch (University of Alabama, Birmingham), and Dr. Scott Simon (UC Davis, CA, USA) for kindly providing cell lines and reagents. This work was supported in part by the National Institutes of Health grants CA97306 and CA-125707, the National Science Foundation grant CBET-0729091, the Johnson & Johnson Innovative Technology, and the PA Dept. of Health Research Fund SAP #41000-26343.

References

1. Alon, R., Chen, S.Q., Puri, K.D., Finger, E.B., Springer, T.A.: The kinetics of L-selectin tethers and the mechanics of selectin-mediated Rolling. J. Cell Biol. **138**, 1169–1180 (1997)
2. Bar-Eli, M.: Role of interleukin-8 in tumor growth and metastasis of human melanoma. Pathobiology **67**, 12–18 (1999)
3. Bell, G.I.: Models for the specific adhesion of cells to cells. Science **200**, 618–627 (1978)
4. Burdick, M.M., McCarty, O.J.T., Jadhav, S., Konstantopoulos, K.: Cell–cell interactions in inflammation and cancer metastasis. IEEE Eng. Med. Biol. Mag. **20**, 86–89 (2001)
5. Cao, J., Donell, B., Deaver, D.R., Lawrence, M.B., Dong, C.: In vitro side-view imaging technique and analysis of human T-leukemic cell adhesion to ICAM-1 in shear flow. Microvasc. Res. **55**, 124–137 (1998)
6. Cassatella, M.A.: The production of cytokines by polymorphonuclear neutrophils. Immunol. Today **16**, 21–6 (1995)
7. Cassatella, M.A.: Neutrophil-derived proteins: selling cytokines by the pound, Adv. Immunol. **73**, 369–509 (1999)
8. Chambers, A.F., MacDonald, I.C., Schmidt, E.E., Morris, V.L., Groom, A.C.: Clinical targets for anti-metastasis therapy. Adv. Cancer Res. **79**, 91–121 (2000)
9. Crawford, S., Belajic, D., Wei, J., Riley, J.P., Dunford, P.J., Bembenek, S., Fourie, A., Edwards, J.P., Karlsson, L., Brunmark, A.: A novel B-RAF inhibitor blocks interleukin-8 (IL-8) synthesis in human melanoma xenografts, revealing IL-8 as a potential pharmacodynamic biomarker. Mol. Cancer. Ther. **7**, 492–499 (2008)
10. Crissman, J.D., Hatfield, J., Schaldenbrand, M., Sloane, B.F., Honn, K.V.: Arrest and extravasation of B16 amelanotic melanoma in murine lungs: a light and EM study. Lab Invest **53**, 470–478 (1985)
11. Dejana, E., Corada, M., Lampugnani, M.G.: Endothelial cell-to-cell junctions, FASEB J **9**, 910–918 (1995)
12. Del Maschio, A., Zanetti, A., Corada, M., Rival, Y., Ruco, L., Lampugnani, M.G., Dejana, E.: Polymorphonuclear leukocyte adhesion triggers the disorganization of endothelial cell-to-cell adherens junctions. J. Cell. Biol. **135**, 497–510 (1996)
13. Dembo, M., Torney, D.C., Saxaman, K., Hammer, D.: The reaction-limited kinetics of membrane-to surface adhesion and detachment. Proc. R. Soc. Lond. **234**, 55–83 (1988)

14. Dong, C., Aznavoorian, S., Liotta, L.A.: Two phases of pseudopod protrusion in tumor cells revealed by a micropipette. Microvasc. Res.**47**, 55–67 (1994)
15. Dong, C., Cao, J., Struble, E., Lipowsky, H.H.: Mechanics of leukocyte deformation and adhesion to endothelium in shear flow. Ann. Biomed. Eng.**27**, 298–312 (1999)
16. Dong, C., Lei, X.: Biomechanics of cell rolling: Shear flow, cell-surface adhesion, and cell deformability. J. Biomechanics **33**, 35–43 (2000)
17. Dong, C., Robertson, G.P.: Immunoediting of leukocyte functions within the tumor microenvironment and cancer metastasis development. Biorheology **46**, 265–279 (2009)
18. Dong, C., Skalak, R.: Leukocyte deformability: finite element modeling of large viscoelastic deformation. J. Theor. Biol. **158**, 173–193 (1992)
19. Dong, C., Skalak, R., Sung, K.L.P., Schmid-Schonbein, G.W., Chien, S.: Passive deformation analysis of human leukocytes. J. Biol. Eng. **110**, 27–36 (1988)
20. Dong, C., Skalak, R., Sung, K.L.P.: Cytoplasmic rheology of passive neutrophils. Biorheology **28**, 557–567 (1991)
21. Dong, C., Slattery, M.J., Liang, S., Peng, H.H.: Melanoma cell extravasation under flow conditions is modulated by leukocytes and endogenously produced interleukin 8. Mol. Cell. Biomech. **2**, 145–159 (2005)
22. Dong, C., Slattery, M.J., Rank, B.M., You, J.: In vitro characterization and micromechanics of tumor cell chemotactic protrusion, locomotion, and extravasation. Ann Biomed Eng **30**, 344–355 (2002)
23. Drury, J.L., Dembo, M.: Aspiration of human neutrophils: effects of shear thinning and cortical dissipation. Biophys. J. **81**, 3166–3177 (2001)
24. Esser, S., Lampugnani, M.G., Corada, M., Dejana, E., Risau, W.: Vascular endothelial growth factor induces VE-cadherin tyrosine phosphorylation in endothelial cells. J. Cell Sci. **111**, 1853–1865 (1998)
25. Frederick, M.J., Clayman, G.L.: Chemokines in cancer. Expert Rev Mol Med. **200**, 1–18 (2001)
26. Giavazzi, R., Foppolo, M., Dossi, R., Remuzzi, A.: Rolling and adhesion of human tumor cells on vascular endothelium under physiological flow conditions. J. Clin. Invest. **92**, 3038–3044 (1993)
27. Gopalan, P.K., Smith, C.W., Lu, H., Berg, E.L., McIntire, L.V., Simon, S.I.: Neutrophil CD18-dependent arrest on intercellular adhesion molecule 1 (ICAM-1) in shear flow can be activated through L-selectin. J. Immunol. **158**, 367–375 (1997)
28. Grutkoski, P.S., Graeber, C.T., Ayala, A., Simms, H.H.: Paracrine suppression of apoptosis by cytokine-stimulated neutrophils involves divergent regulation of NF-kappaB, Bcl-X(L), and Bak, Shock **17**, 47–54 (2002)
29. Hentzen, E.R., Neelamegham, S., Kansas, G.S., Benanti, J.A., McIntire, L.V., Smith, C.W., Simon, S.I.: Sequential binding of CD11a/CD18 and CD11b/CD18 defines newtuophil capture and stable adhesion to intercellular adhesion molecule-1. Blood **95**, 911–920 (2000)
30. Hodgson, L., Dong, C.: [Ca^{2+}] as a potential down regulator of $\alpha_2\beta_1$ integrin-mediated A2058 tumor cell migration to type IV collagen. Am. J. Physiol. Cell Physiol. **281**, C106–C113 (2001)
31. Hodgson, L., Henderson, A.J., Dong, C.: Melanoma cell migration to type IV collagen requires activation of NF-kappaB. Oncogene **22**, 98–108 (2003)
32. Holmes, W.E., Lee, J., Kuang, W.J., Rice, G.C., Wood, W.I.: Structure and functional expression of human interleukin-8 receptor. Science **253**, 1278–1280 (1991)
33. Hoskins, M.H., Dong, C.: Kinetics analysis of binding between melanoma cells and neutrophils. Mol. Cell Biomech. **3**, 79–87 (2006)
34. Hoskins, M.H., Kunz, R.F., Bistline, J., Dong, C.: Coupled flow-structure-biochemistry simulations of dynamic systems of blood cells using an adaptive surface tracking method. J. Fluids Struct. **25**, 936–953 (2009)
35. House, S., Lipowsky, H.: In vivo determination of the force of leukocyte-endothelium adhesion in the mesenteric microvasculature of the cat. Circ. Res. **63**, 658–668 (1988)

36. Huh, S.J., Liang, S., Sharma, A., Dong, C., Robertson, G.P.: Transiently entrapped circulating tumor cells interact with neutrophils to facilitate lung metastasis development. Cancer Res. **70**, 6071–6082 (2010)
37. Jadhav, S., Eggleton, C.D., Konstantopoulos, K.: A 3-D computational model predicts that cell deformation affects selectin-mediated leukocyte rolling. Biophys. J. **88**, 96–104 (2005)
38. Jadhav, S., Konstantopoulos, K.: Fluid shear- and time-dependent modulation of molecular interactions between PMNs and colon carcinomas. Am. J. Physiol. Cell Physiol. **283**, C1133–C1143 (2002)
39. Khanna, P., Yunkunis, T., Muddana, H.S., Peng, H.H., August, A., Dong, C.: p38 MAP kinase is necessary for melanoma-mediated regulation of VE-cadherin disassembly. Am. J. Physiol. Cell Physiol. **298,** C1140–C1150 (2010)
40. Khismatullin, D., Truskey, G.: Three-dimensional numerical simulation of receptor-mediated leukocyte adhesion to surfaces: Effects of cell deformability and viscoelasticity. Phys. Fluids. **17**, 031505-1–21 (2005)
41. Konstantopoulos, K., Thomas, S.N.: Cancer cells in transit: the vascular interactions of tumor cells. Annu. Rev. Biomed. Eng. **11**, 177–202 (2009)
42. Kooijman, H.A.: A modification of the Stokes–Einstein equation for diffusivities in dilute binary mixtures. Ind. Eng. Chem. Res. **41**, 3326–3328 (2002)
43. Kramer, R.H., Nicolson, G.L.: Interactions of tumor cells with vascular endothelial cell monolayers: a model for metastatic invasion. Proc. Natl. Acad. Sci. USA **76**, 5704–5708 (1979)
44. Kunz, R.F., Yu, W.S., Antal, S.P., Ettorre, S.M.: An unstructured two-fluid method based on the coupled phasic exchange algorithm. AIAA Paper # AIAA-2001-2672. In: AIAA Computational Fluid Dynamics Conference, 15th, Anaheim, June 11–14, (2001)
45. Lampugnani, M.G., Corada, M., Caveda, L., Breviario, F., Ayalon, O., Geiger, B., Dejana, E.: The molecular organization of endothelial cell to cell junctions: differential association of plakoglobin, beta-catenin, and alpha-catenin with vascular endothelial cadherin (VE-cadherin). J. Cell Biol. **129**, 203–217 (1995)
46. Lei, X., Lawrence, M.B., Dong, C.: Influence of cell deformation on leukocyte rolling adhesion in shear flow. J. Biomech. Eng. **121**, 636–643 (1999)
47. Leyton-Mange, J., Sung, Y., Henty, M., Kunz, R.F., Zahn, J., Dong, C.: Design of a side-view particle imaging velocimetry flow system for cell-substrate adhesion studies. J. Biomech. Eng **128**, 271–278 (2006)
48. Liang, S., Dong, C.: Integrin VLA-4 enhances sialyl-Lewisx/a-negative melanoma adhesion to and extravasation through the endothelium under low flow conditions. Am. J. Physiol. Cell. Physiol. **295**, C701–707 (2008)
49. Liang, S., Fu, C., Wagner, D., Guo, H., Zhan, D., Dong, C., Long, M.: 2D kinetics of β_2 integrin-ICAM-1 bindings between neutrophils and melanoma cells. Am. J. Physiol. **294**, C743–C753 (2008a)
50. Liang, S., Hoskins, M.H., Dong, C.: Tumor cell extravasation mediated by leukocyte adhesion is shear rate-dependent on IL-8 signaling. Mol. Cell. Biomech. **7**(2), 77–91 (2009)
51. Liang, S., Hoskins, M.H., Khanna, P., Kunz, R.F., Dong, C.: The tumor-leukocyte microenvironment in a shear flow and how it affects melanoma–neutrophil adhesion to the endothelium. Cell. Mol. Bioeng. **1**, 189–200 (2008b)
52. Liang, S., Sharma, A., Peng, H.H., Robertson, G., Dong, C.: Targeting mutant (V600E) B-Raf in melanoma interrupts immunoediting of leukocyte functions and melanoma extravasation. Cancer Res **67**, 5814–5820 (2007)
53. Liang, S., Slattery, M., Dong, C.: Shear stress and shear rate differentially affect the multi-step process of leukocyte-facilitated melanoma adhesion. Exp. Cell Res. **310**, 282–292 (2005)
54. Liang, S., Slattery, M.J., Wagner, D., Simon, S.I., Dong, C.: Hydrodynamic shear rate regulates melanoma–leukocyte aggregation, melanoma adhesion to the endothelium, and subsequent extravasation. Ann. Biomed. Eng. **36**, 661–671 (2008c)
55. Liao, F., Doody, J.F., Overholser, J., Finnerty, B., Bassi, R., Wu, Y., Dejana, E., Kussie, P., Bohlen, P., Hicklin, D.J.: Selective targeting of angiogenic tumor vasculature by vascular

endothelial-cadherin antibody inhibits tumor growth without affecting vascular permeability. Cancer Res. **62**, 2567–2575 (2002)
56. Liotta, L.A.: Cancer cell invasion and metastasis. Sci. Am. **266**, 54–63 (1992)
57. Lynam, E., Sklar, L.A., Taylor, A.D., Neelamegham, S., Edwards, B.S., Smith, C.W., Simon, S.I.: Beta2-integrins mediate stable adhesion in collisional interactions between neutrophils and ICAM-1-expressing cells. J. Leukoc. Biol. **64**, 622–630 (1998)
58. Ma, Y.P., Wang, J., Liang, S., Dong, C., Du, Q.: Application of population dynamics to study heterotypic cell aggregations in the near-wall region of a shear flow. Cell. Mol. Bioeng. **3**(1), 3–19 (2010)
59. Marie, C., Roman-Roman, S., Rawadi, G.: Involvement of mitogen-activated protein kinase pathways in interleukin-8 production by human monocytes and polymorphonuclear cells stimulated with lipopolysaccharide or mycoplasma fermentans membrane lipoproteins. Infect. Immun. **67**, 688–693 (1999)
60. Miele, M.E., Bennett, C.F., Miller, B.E., Welch, D.R.: Enhanced metastatic ability of TNF-treated maliganant melanoma cells is reduced by intercellular adhesion molecule-1 (ICAM-1) antisense oligonucleotides. Exp. Cell Res. **214**, 231–241 (1994)
61. Migliorini, C., Qian, Y.H., Chen, H.D., Brown, E.B., Jain, R.K., Munn, L.L.: Red blood cells augment leukocyte rolling in a virtual blood vessel. Biophys. J. **83**, 1834–1841 (2002)
62. Moghe, P.V., Nelson, R.D., Tranquillo, R.T.: Cytokine-stimulated chemotaxis of human neutrophils in a 3-D conjoined fibrin gel assay. J. Immunol. Meth. **180**, 193–211 (1995)
63. Muller, A., Homey, B., Soto, H., Ge, N., Catron, D., Buchanan, M.E., McClanahan, T., Murphy, E., Yuan, W., Wagner, S.N., Barrera, J.L., Mohar, A., Verastegui, E., Zlotnik, A.: Involvement of chemokine receptors in breast cancer metastasis. Nature **410**, 50–6 (2001)
64. Munn, L.L., Melder, R.J., Jain, R.K.: Analysis of cell flux in the parallel plate flow chamber: implications for cell capture studies. Biophys. J. **67**, 889–895 (1994)
65. Murphy, P.M., Tiffany, H.L.: Cloning of complementary DNA encoding a functional human interleukin-8 receptor. Science **253**, 1280–1283 (1991)
66. N'Dri, N.A., Shyy, W., Tran-Son-Tay, R.: Computational modeling of cell adhesion and movement using a continuum-kinetics approach. Biophys. J. **85**, 2273–2286 (2003)
67. 'Neelamegham, S.: Transport features, reaction kinetics and receptor biomechanics controlling selectin and integrin mediated cell adhesion. Cell Commun. Adhes. **1**, 35–50 (2004)
68. Neelamegham, S., Taylor, A.D., Burns, A.R., Smith, C.W., Simon, S.I.: Hydrodynamic shear shows distinct roles for LFA-1 and MAC-1 in neutrophil adhesion to intercellular adhesion molecule-1. Blood **72**, 1626–1638 (1998)
69. Nwariaku, F.E., Chang, J., Zhu, X., Liu, Z., Duffy, S.L., Halaihel, N.H., Terada, L.: Turnage RH The role of p38 map kinase in tumor necrosis factor-induced redistribution of vascular endothelial cadherin and increased endothelial permeability. Shock **1**, 82–5 (2002)
70. Okamoto, M., Liu, W., Luo, Y., Tanaka, A., Cai, X., Norris, D.A., Dinarello, C.A., Fujita, M.: Constitutively active inflammasome in human melanoma cells mediating autoinflammation via caspase-1 processing and secretion of interleukin-1β. J. Biol. Chem. **285,** 6477–6488 (2010)
71. Payne, A.S., Cornelius, L.A.: The role of chemokines in melanoma tumor growth and metastasis. J. Invest. Dermatol. **118**, 915–922 (2002)
72. Peng, H.H., Dong, C.: Systemic analysis of tumor cell-induced endothelial calcium signaling and junction disassembly. Cell. Mol. Bioeng. **2**(3), 375–385 (2009)
73. Peng, H.H., Hodgson, L., Henderson, A.J., Dong, C.: Involvement of phospholipase C signaling in melanoma cell-induced endothelial junction disassembly. Frontiers Biosci. **10**, 1597–1606 (2005)
74. Peng, H.H., Liang, S., Henderson, A.J., Dong, C.:Regulation of interleukin-8 expression in melanoma-stimulated neutrophil inflammatory response. Exp. Cell Res. **313**, 551–559 (2007)
75. Qi, J., Chen, N., Wang, J., Siu, C.H.: Transendothelial migration of melanoma cells involves N-cadherin-mediated adhesion and activation of the beta-catenin signaling pathway. Mol. Biol. Cell. **16**, 4386–4397 (2005)

76. Rinker, K.D., Prabhakar, V., Truskey, G.A.: Effect of contact time and force on monocyte adhesion to vascular endothelium. Biophys. J. **80**, 1722–1732 (2001)
77. Sandig, M., Voura, E.B., Kalnins, V.I., Siu, C.H.: Role of cadherins in the transendothelial migration of melanoma cells in culture. Cell Motil Cytoskelet. **38**, 351–64 (1997)
78. Schadendorf, D., Mohler, T., Haefele, J., Hunstein, W., Kelholz, U.: Serum interleuckin-8 is elevated in patients with metastatic melanoma and correlates with tumor load. Melanoma Res. **5**, 179–181 (1995)
79. Scherbarth, S., Orr, F.W.: Intravital video microscopic evidence for regulation of metastasis by the hepatic microvasculature: Effects of interleukin-1 on metastasis and the location of B16F1 melanoma cell arrest. Cancer Res. **57**, 4105–4110 (1997)
80. Sharma, A., Tran, M., Liang, S., Sharma, A.K., Amin, S., Smith, C.D., Dong, C., Robertson, G.P.: Targeting mitogen-activated protein kinase/extracellular signal-regulated kinase kinase in the mutant (V600E) B-Raf signaling cascade effectively inhibits melanoma lung metastases. Cancer Res. **66**, 8200–8209 (2006)
81. Shay-Salit, A., Shushy, M., Wolfovitz, E., Yahav, H., Breviario, F., Dejana, E., Resnick, N.: VEGF receptor 2 and the adherens junction as a mechanical transducer in vascular endothelial cells. Proc. Natl. Acad. Sci. USA **99**, 9462–9427 (2002)
82. Simon, S.I., Green, C.E.: Molecular mechanics and dynamics of leukocyte recruitment during inflammation. Annu. Rev. Biomed. Eng. **7**, 151–185 (2005)
83. Singh, R.K., Gutman, M., Radinsky, R., Bucana, C.D., Fidler, I.J.: Expression of interleukin 8 correlates with the metastatic potential of human melanoma cells in nude mice. Cancer Res. **54**, 3242–3247 (1994)
84. Singh, R.K., Varney, M.L.: Regulation of interleukin-8 expression in human malignant melanoma cells. Cancer Res.**58**, 1532–1537 (1998)
85. Singh, S., Varney, M., Singh, R.K.: Host CXCR2-dependent regulation of melanoma growth, angiogenesis, and experimental lung metastasis. Cancer Res. **69**, 411–5 (2009)
86. Slattery, M.J., Dong, C.: Neutrophils influence melanoma adhesion and migration under flow conditions. Int. J. Cancer **106**, 713–722 (2003)
87. Slattery, M.J., Liang, S., Dong, C.: Distinct role of hydrodynamic shear in leukocyte-facilitated tumor cell extravasation. Am. J. Physiol. Cell Physiol. **288**(4), C831–839 (2005)
88. Smith, M.J., Berg, E.L., Lawrence, M.B.: A direct comparison of selectin-mediated transient, adhesive events using high temporal resolution. Biophys. J. **77**, 3371–3383 (1999)
89. Springer, T.A.: Traffic signals for lymphocyte recirculation and leukocyte emigration: the multistep paradigm. Cell **76**, 301–314 (1994)
90. Starkey, J.R., Liggitt, H.D., Jones, W., Hosick, H.L.: Influence of migratory blood cells on the attachment of tumor cells to vascular endothelium. Int. J. Cancer **34**, 535–543 (1984)
91. Strieter, R.M., Kasahara, K., Allen, R.M., Standiford, T.J., Rolfe, M.W., Becker, F.S., Chensue, S.W., Kunkel, S.L.: Cytokine-induced neutrophil-derived interleukin-8. Am. J. Pathol. **141**, 397–407 (1992)
92. Thorlacius, H., Pricto, J., Raud, J., Gautam, N., Patarroyuo, M., Hedqvist, P., Lindbom, L.: Tumor cell arrest in the microcirculation: lack of evidence for a leukocyte-like rolling adhesive interaction with vascular endothelium in vivo. Clin. Immunol. Immunopathol. **83**, 68–76 (1997)
93. Todaro, G.J., Fryling, C., De Larco, J.E.: Transforming growth factors produced by certain human tumor cells: polypeptides that interact with epidermal growth factor receptors. Proc. Natl. Acad. Sci. USA **77**, 5258–62 (1980)
94. Tominaga, Y., Kita, Y., Satoh, A., Asai, S., Kato, K., Ishikawa, K., Horiuchi, T., Takashi, T.: Affinity and kinetic analysis of the molecular interaction of ICAM-1 and leukocyte function-associated antigen-1. J. Immunol. **161**, 4016–4022 (1998)
95. Tremblay, P.L., Auger, F.A., Huot, J.: Regulation of transendothelial migration of colon cancer cells by E-selectin-mediated activation of p38 and ERK MAP kinases. Oncogene **25**, 6563–73 (2006)
96. Van Wetering, S., van den Berk, N., van Buul, J.D., Mul, F.P., Lommerse, I., Mous, R., ten Klooster, J.P., Zwaginga, J.J., Hordijk, P.L.: VCAM-1-mediated Rac signaling controls

endothelial cell–cell contacts and leukocyte transmigration. Am. J. Physiol. Cell Physiol. **285**, 343–352 (2003)
97. Vitte, J., Pierres, A., Benoliel, A.M., Bongrand, P.: Direct quantification of the modulation of interaction between cell- or surface-bound LFA -1 and ICAM-1. J. Leukoc. Biol. **76**, 1–9 (2004)
98. Volberg, T., Zick, Y., Dror, R., Sabanay, I., Gilon, C., Levitzki, A., Geiger, B.: The effect of tyrosine-specific protein phosphorylation on the assembly of adherens-type junction. EMBO J. **11**, 1733–1742 (1992)
99. Voura, E.B., Sandig, M., Siu, C.H.: Cell–cell interactions during transendothelial migration of tumor cells. Microsc Res Tech. **43**, 265–275 (Review) (1998)
100. Walz, A., Peveri, P., Aschauer, A.O., Baggiolini, M.: Purification and amino acid sequencing of NAF, a novel neutrophil activating factor produced by monocytes. Biochem. Biophys. Res. Commun **149**, 755–761 (1987)
101. Welch, D.R., Bisi, J.E., Miller, B.E., Conaway, D., Seftor, E.A., Yohem, K.H., Gilmore, L.B., Seftor, R.E.B., Nakajima, M., Hendrix, M.J.C.: Characterization of a highly invasive and spontaneously metastatic human malignant melanoma cell line. Int. J. Cancer **47**, 227–237 (1991)
102. Welch, D.R., Schissel, D.J., Howrey, R.P., Aeed, P.A.: Tumor-elicited polymorphonuclear cells, in contrast to "normal" circulating polymorphonuclear cells, stimulate invasive and metastatic potentials of rat mammary adnocardinoma cells. Proc. Natl. Acad. Sci. USA **86**, 5859–5863 (1989)
103. Yamada, K.M.: Introduction: Adhesion molecules in cancer. Part I. Semin. Cancer Biol. **4**, 215–218 (1993)
104. Yeung, A., Evans, E.: Cortical shell-liquid core model for passive flow of liquid-like spherical cells into micropipets. Biophys. J. **56**, 139–149 (1989)
105. You, J., Mastro, A.M., Dong, C.: Application of the dual micropipette technique to the measurement of tumor cell locomotion. Exp. Cell Res. **248**, 160–171 (1999)
106. You, J., Miele, M.E., Dong, C., Welch, D.R.: Suppression of human melanoma metastasis by introduction of chromosome 6 may be partially due to inhibition of motility but not invasion. Biochem. Biophys. Res. Commun. **208**, 476–484 (1995)
107. Young, M.E., Carroad, P.A., Bell, R.L.: Estimation of diffusion coefficients of proteins. Biotechnol. Bioeng. **22**, 947–955 (1980)
108. Zetter, B.R.: Adhesion molecules in tumor metastasis. Semin. Cancer Biol. **4**, 219–229 (1993)
109. Zhang, X.H., Wojcikiewicz, E., Moy, V.: Force spectroscopy of the leukocyte function-associated antigen-1/intercellular adhesion molecule-1 interaction. Biophys. J. **83**, 2270–2279 (2002)
110. Zhu, C., Yago, T., Lou, J., Zarnitsyna, V.I., McEver, R.P.: Mechanisms for flow-enhanced cell adhesion. Ann. Biomed. Eng. **36**, 604–621 (2008)